Chemical Engineering Journal 452 (2023) 139098

Contents lists available at ScienceDirect

Chemical Engineering Journal

journal homepage: www.elsevier.com/locate/cej

Review

Deciphering exogenous electric field promoting catalysis from the perspectives of electric energy and electron transfer: A review

Ziang Zhang [a,b], Caiting Li [a,b,*], Xueyu Du [a,b], Youcai Zhu [a,b], Le Huang [a,b], Kuang Yang [a,b], Jungang Zhao [a,b], Caixia Liang [a,b], Qi Yu [a,b], Shanghong Li [a,b], Xuan Liu [a,b], Yunbo Zhai [a,b]

[a] College of Environmental Science and Engineering, Hunan University, Changsha 410082, PR China
[b] Key Laboratory of Environmental Biology and Pollution Control (Hunan University), Ministry of Education, Changsha 410082, PR China

ARTICLE INFO

Keywords:
Electric field promoting catalysis
Harmful gas abatement
Chemical and fuel production
Electric energy
Electron transfer

ABSTRACT

A synergistic system of the non-intense electric field incorporated in semiconductor catalysts has drawn growing attention as an advanced method to promote cryogenic catalytic activity and to satisfy demanding requirements for specific reactions in recent years. Despite the considerable potential for addressing the energy dilemma and atmospheric environment pollution, it lacks a comprehensive review to elucidate the process and mechanism in this research field. Herein, a critical discussion of classification is provided on the research progress of exogenous electric field promoting catalysis in terms of application categories, including production of fuel or chemical feed gases (methane oxidative coupling, methane steam reforming, ammonia synthesis), and abatement of harmful gases (oxidation of lean methane and VOCs). Then, a shared mechanism framework for this field is constructed preliminarily with a core of electric energy and electron transfer, deriving the characteristic phenomena and merits in this catalytic system. Finally, further research suggestions on electric field promoting catalysis comprising scope expanding of research and application, mechanism imperfections filling, and evaluative indicators establishment, which contribute to the development and commercialization of this technology.

1. Introduction

The last decades have witnessed pressing energy and environmental issues from anthropogenic activities, including resource depletion, multiphase pollution, and climate deterioration [1–5]. However, energy & resources are essential for many processes at a stake of human development [6], especially chemical synthesis and fuel production. No doubt that a wide range of reactions can be carried out efficiently by catalytic collaborations to meet given demanding requirements, such as the specific reaction temperature, the conversion rate, and the selectivity [7–9]. Accordingly, the researchers struggled to modify catalysts and try incorporating exogenous fields and energy into catalytic systems to enhance catalytic capacities [10], such as electric fields (electrocatalysis) [11–13], light (photocatalysis) [14,15], magnetic field (microwave catalysis) [16], and hybrid fields [17–19] (photothermal, electrothermal, and photoelectric catalysis, etc.).

Among the exogenous energy, electricity has been subjected as a mature power source for the stable triggering and control, with typical catalytic synergy forms of Non-thermal plasma (NTP), Faraday electrolysis, and non-Faraday electrocatalysis (NEMCA). NEMCA facilitates the reaction by loading weak voltage (<5 V) over electrolytes (anionic and cationic conductors) to pump out and in carriers to the metal catalyst surface, but requires severe temperature conditions (even up to 900 K) [20]. Recently, plasma-assisted catalytic technology has been proposed as alternative strategy, with various discharge types including of dielectric barrier (DBD) [21,22], glow [23], corona [24], and radio frequency (RF) [25,26]. In plasma catalysis, high-energy electrons bombard the ground state molecules (O_2, N_2), turning them into metastable (O^m, N^m) or excited (O*, N*) [27,28]. Through multistaged physical and chemical reactions, reactive oxygen species (ROS), such as ·OH, H_2O_2, and NO, are formed and react with gaseous contaminants (Fig. 1a). The ultra-high voltages required for dielectric breakdown and molecules ionization cause essential energy consumption, while complicated interactions between reactive species introduce the hazardous intermediates inevitably.

A more lenient system to implement electricity incorporation has been applied to multiple gas-phase catalytic reactions, introducing an adequate EF (electric field strength is of the order of 10^5 V/m, between

* College of Environmental Science and Engineering, Hunan University, Changsha 410082, PR China
E-mail addresses: ziang_mengjie@163.com (Z. Zhang), ctli@hnu.edu.cn (C. Li).

https://doi.org/10.1016/j.cej.2022.139098
Received 5 April 2022; Received in revised form 29 August 2022; Accepted 5 September 2022
Available online 8 September 2022

plasma and NEMCA) into polarizing and activating heterogeneous catalyst at low temperature [29]. The electrochemical process of this electric field promoting catalytic system is similar to NEMCA (non-Faraday electrocatalysis), while its system setup is closer to that of plasma. This EF assisted the catalyst activation (promotion of oxygen vacancies or lattice strain) through direct electron transport, [30] and avoided the energy consumption for generation of high-energy electrons and ROS in NTP. Most researchers illustrated the mechanism in terms of surface proton hopping [31–33] or electron transport [34], some of which also glimpsed at the factors of charged adsorption [35,36], electric heating and lattice strain. Previous reviews on the EF promoting catalytic systems is mainly in the application of energy and chemical field [7–9], lacking of latest research for atmospheric environment. The rapid development of this system requires a comprehensive updated assessment.

Here, we recapitulate electric field promoting catalysis orderly, taking application categories as the discussed thread. It highlights the latest research direction of Health & Environment, the catalytic oxidation of dilute greenhouse gases and VOCs. We commit to integrating various reactions into a shared mechanism framework. The ultimate objective of this review is to provide a fundamental framework, frontier theories, research routes that contribute to the study of EF promoting catalysis to support sustainable energy production and efficient pollutant removal.

2. General description

2.1. Reaction system and setup

A typical setup of electrical field promoting catalysis are shown in Fig. 1b, including the power supply module, catalytic reaction module, and gas circuit [37–42]. The catalytic module is established on the conventional fixed-bed catalytic reactor, in which two-section metal electrodes are attached coaxially on both ends of the catalyst. Unlike plasma discharge where the dielectric of gaseous or solid exists between the catalyst and the electrode (Fig. 1a), electrons move into and out of the catalytic bed directly by the metal electrodes on both sides and migrate in the intermediate semiconductor in this system. In some instances, the catalyst surface was covered with a conductive material layer (e.g., foam sheet metal) to reduce contact resistance [37,43]. In the laboratory operations, the catalytic heat is supplied by a thermoelectric furnace, and monitored by a connected thermocouple, thus mastering the heating effect on the reaction results. The catalytic activity and selectivity were fundamental indicators obtained through the quantitative measurement, such as gas chromatography hydrogen flame ionization detector (GC-FID), gas chromatography thermal conductivity detectors (GC-TCD), and ion chromatography (IC).

2.2. Catalysts conductivity and energy consumption

Conventional catalyst selections typically depend on activity, selectivity, temperature suitability, lifetime, and recyclability [44]. In

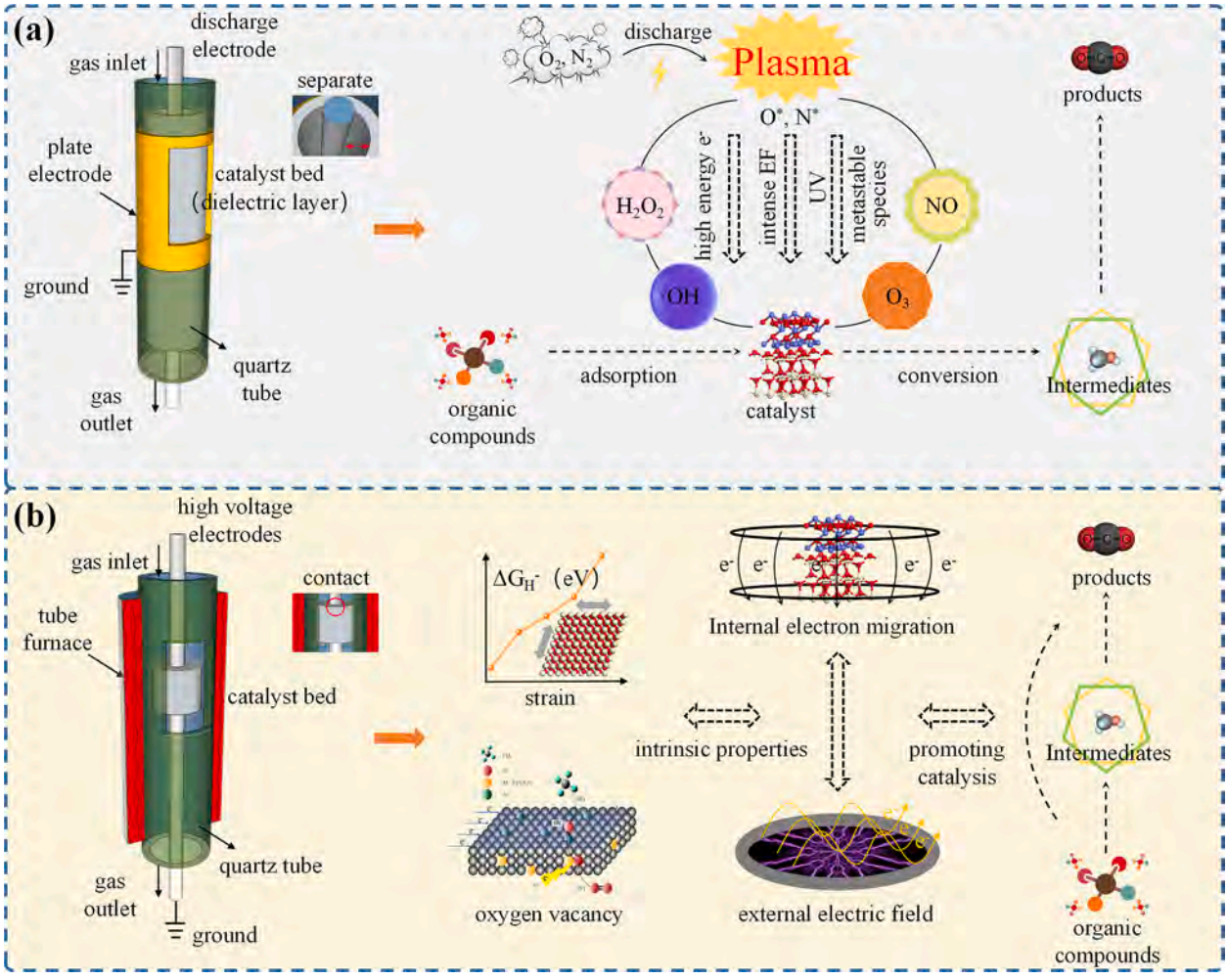

Fig. 1. Comparison of basic processes and system set-up for plasma-assisted catalysis (DBD discharge) and electric field promoted catalysis.

electric field promoting catalytic reactions, additional consideration is given to the intrinsic conductivity, or rather to the capability of proton and electron migration [45,46]. It summarizes the catalysts used in previous reports (Table 1) of electric field promoting catalysis, mainly ceramic semiconductors of various synthesis methods.

Semiconductor materials with a spacious forbidden-band width possess their strong capability of valence electron binding [47–49], resulting in a non-negligible resistivity. Based on the "Grotthuss mechanism", Sakai et al. concluded that candidates of semiconductor supporters in this system should contribute to activity and be non-insulating to maintain surface proton current [50]. Overly faint electrical conductivity caused spark discharge instead of proton hopping or electron transfer, thus reducing the energy efficiency. The centralized selections were in this system of the calcium fluoride structure as CeO_2 and ZrO_2 [37–39,41,51–54], spinel crystal structure as Co_3O_4 [55–59], and perovskites as $LaALO_3$, $SrAlO_3$, $SrZrO_3$ [40,60–62].

Electronic/protonic conductivity within dry and wet conditions was tested by electrochemical impedance spectroscopy (EIS) measurement [63]. The interaction between moisture and catalyst conductivity stem from sequential proton hopping via the hydrogen bonding of H_2O molecular [64–66]. Under dry conditions, the conductivity is proportional to the temperature derived from the electronic thermal diffusion of inner bulk (volume conductivity). The adsorbate of water or chemical groups triggered surface proton conductivity in a humid condition (Eq. (1)), wet conductivity (σ_{wet}) summed from volume conductivity (σ_{dry}), and surface proton conductivity (σ_{H+}) [63,67].

$$\sigma_{wet} = \sigma_{dry} + \sigma_{H^+} \quad (1)$$

EF promoting catalytic reaction system has low power consumption and high reaction adaptability, typically no >10 W in previous studies as in Table 1, while plasma-assisted catalysis >100 W under similar reaction conditions. The power consumption originates from two parts, reaction consumption and thermal release (Joule heat). This semiconductor resistance caused energy dissipation to surroundings and changed the ambient temperature, which influenced activity test indicators. A series of more precise measurements were applied to assuring the Joule heat implications on catalytic system temperature [31,68,69]. Among them, the X-ray absorption fine structure (EXAFS) analysis with temperature factor (DWF), closed to realistic assessment, indicated the electricity leading to a <50 K temperature rising over Pd catalytic surface at an ambient temperature of 473 K [68].

Table 1
Power parameters of EF promoting catalysis and plasma-assisted catalysis.

Reaction	Catalysts		EF parameter			Reaction condition	Ref.
	Category	Synthesis method	I mA	U_{peak} kV	P_{peak} W		
Catalytic oxidation	$Co_3O_4Ce_{0.75}Zr_{0.25}$[a]	Solution combustion	9	0.30	2.7	0.2 % CH_4, 10 % O_2, N_2 balanced	[37]
	$Mn_1Co_5O_x$[a]	SHS[c]	20	0.25	4.9	0.2 % CH_4, 1 % O_2, N_2 balanced	[58]
	$Pd/Ce_{0.75}Zr_{0.25}O_x$[a]	FSP[d]	3	0.33	1.0	0.2 % CH_4, 10 % O_2, N_2 balanced	[51]
	Pd/Co_3O_4[a]	SHS	100	0.08	8.0	0.2 % CH_4, 1 % O_2, N_2 balanced	[56]
Oxidative coupling	nanorod $CePO_4$[a]	hydrothermal	7	0.31	2.2	CH_4 = 15 mL min^{-1} O_2 = 12 mL min^{-1} Ar = 33 mL min^{-1}	[119]
	Sr-La_2O_3[a]	Citric acid	7	0.50	3.5	CH_4 = 25 mLmin^{-1} O_2 = 5 mL min^{-1} Ar = 100 mL min^{-1}	[40]
	10 % La-ZrO_2[a]	complex polymerized	3	0.21	6.3	CH_4 = 25 mL min^{-1} CO_2 = 25 mL min^{-1} Ar = 50 mL min^{-1}	[62]
	Cu/γ-Al_2O_3[b]	impregnation	/	22	18	CH_4 = 25 mL min^{-1} O_2 = 5 mL min^{-1} He = 30 mL min^{-1}	[24]
Steam reforming	$Rh/Ce_{0.25}Zr_{0.75}O_2$[a]	impregnation	3	0.12	3.5	CH_4 = 12 mL min^{-1} H_2O = 24 mL min^{-1} Ar = 18 mL min^{-1}	[42]
	Rh/CeO_2[a]	impregnation	3	0.67	2.0	C_2H_5OH = 0.5 mmol min^{-1} H_2O = 0.5 mmolmin^{-1} Ar = 20 mL min^{-1}	[133]
	Ni/CeO_2[b]	impregnation	/	0.15	500	10 wt% glycerol 3.0 mL/h flow rate WHSV = 15 h^{-1}	[23]
Synthetic ammonia	$Ru/SrZrO_3$[a]	impregnation	6	0.47	2.8	N_2 = 60 mL min^{-1} H_2 = 180 mL min^{-1}	[31]
	Ni/Al_2O_3[b]	impregnation	/	24	450	N_2 = 50 mL min^{-1} H_2 = 100 mL min^{-1}	[26]
Dry reforming	Ni/La-ZrO_2[a]	complex polymerized	3	0.12	3.7	CH_4 = 25 mL min^{-1} CO_2 = 25 mL min^{-1} Ar = 50 mL min^{-1}	[39]
	La_2O_3-$MgAl_2O_4$[b]	impregnation	/	/	100	CH_4 = 10 mL min^{-1} CO_2 = 10 mL min^{-1} He = 30 mL min^{-1}	[21]

[a] for EF promoting catalysis.
[b] for plasma-assisted catalysis.
[c] SHS: self-propagating high-temperature synthesis.
[d] FSP: flame spray pyrolysis synthesis.

2.3. Research development

Research on electric field promoting catalysis was performed through experiment and theoretical calculation. The main events and time points for progress of EF promoting catalysis are shown in Fig. 2. As soon as proposed was this novel hybrid process of an electric field and catalysts, the fundamental catalytic system architecture was going to be established by Sekine et al. The Pt/CeO_2 catalyst synthesized by impregnation was first applied to the decomposition of ethanol in EF [29]. Taking into the advantages of low reaction temperature and energy consumption, this catalytic system was operated experimentally into the ammonia synthesis [31], methane (steam/dry) reforming [39,42], and methane oxidative coupling [62], and water gas shift [41] immediately.

As global environmental issues stand out, researchers have been turning their attention to EF promoting catalytic oxidation of hazard gases and greenhouse gases, including dilute methane, carbon dioxide, and VOCs. Lin et al. revolved around the additive role of electric field on the active component (Pd, Pt, Cu, etc.) and high redox capacity support (CeO_2) and manifested its low-temperature activity and catalytic subsidiarity. Furthermore, the theoretical calculations drawn from density functional theory (DFT) and molecular dynamics (MD) speculated for the decline of dissociation or adsorption energy [35,36], mitigation of activation barrier [73], and advance of the reaction step [74] in an electric field, which closely corresponds to experiments. Other reactions in EF were occasionally reported, methylcyclohexane dehydrogenation [33,70], CO degradation of modified graphene [71], and dimethyl ether (DME) hydrolysis [72]. It is necessary to distinguish the selective electrostatic catalysis oriented external electric fields (OEEFs) and the EF promoting catalysis, the former was not involved in this review for inconsistencies on catalyst level, electric field strength (at least 10^7 V m^{-1}), and micro-mechanics. This system trigger charge segregation of considerable dipole-moment on single-molecule catalysis [75–77].

3. EF promoting catalysis for harmful gases abatement

3.1. EF promoting dilute methane catalytic oxidation

Methane is one of the typical combustion models for oxidation retardancy by stable tetrahedral structure (CH_3-H bond of 431.8 kJ mol^{-1}) [78,79]. Bulk stored in natural gas, the methane share of about 85 % volume [80]. Methane utilization can reduce emissions of sulfur oxides, nitrogen oxides, and dust, but the emission of lean methane from some anthropogenic sources has become a significant culprit of the greenhouse effect, as the natural gas vehicle exhaust [81] and coal-mining ventilation air (8 % anthropogenic CH_4 source) [82–85]. More seriously, the global warming potential of CH_4 attains 23 times higher than CO_2 [86].

Catalytic combustion of CH_4 (CCM) as a proposed technology, was utilized predominantly over noble metal catalysts supported by ceramic semiconductors (oxides of cobalt (Co) [87], alumina (Al) [88], zirconia (Zr) [89,90] and ceria (Ce)) [91] and minority in non-precious metal catalyst [92,93]. Although precious metal dopant enhanced reaction activity, the completely converted methane (1 %) still required a demanding temperature of 350 °C (300 °C over Pd/CeO_2 catalysts with deactivation after 16 h [94]). More laboriously, the ultra-dilute methane (<1%) catalytic combustion needs higher thermal energy, Ercolino et al. [95] achieved a complete conversion temperature of 450 °C for 0.5 % methane over Pd/Co_3O_4 catalysts by optimizing preparation methods. Cargnello et al. [96] reduced the temperature to 400 °C using a core–-shell catalysts (Pd–Ce–Al).

In recent years, Lin et al. incorporated an external electric field into the ultra-lean methane (0.1 %) catalytic oxidation, achieving a excellent conversion at low temperatures. In similar conditions, the conversion ratios over noble metal [55,56,97] and non-noble metal [37,58] in the EF were both considerable, light-off temperature (T_{50}) lower than 275 °C, and near-complete complete oxidation (T_{90}) lower than 350 °C (Fig. 3a,d). Compared with conventional catalytic combustion, the system approximately achieves a 100 °C drop in the complete conversion temperature. Reduction of the activation energy (from 55.9 kJ mol^{-1} to 28.1 kJ mol^{-1}) by inputting current was more salient than by increasing Pd loading ratio, supposed to be the apparent reason for the decline of light-off temperature [97].

The EF incorporation did not disrupt the activity order for different metal-doped ratio conditions (Fig. 3a,d), in turn, this ratio influenced the EF facilitating effect to some extent. For the Mn_xO_y catalyst of Mn/Co > 1, the electric field positive role for catalysis was almost invisible (Fig. 3a). In such conditions, Co was dispersed well into Mn_3O_4 and no CoO or Co_3O_4 phase was observed [58]. In HRTEM images (Fig. 3c), different from a sole Mn_3O_4 lattice fringe on Mn/Co > 1, the lattice fringe of CoO (1 1 1) planes was observed on treated Mn/Co < 1 with 0.201 nm d spacing. Both theoretical and experimental results indicated the formation of CoO lattice is inseparable for this catalytic enhancement of EF. As shown in Fig. 3b, the electric field drives the shift of ionic equilibrium between Co species and Mn species, which promotes the generation of additional octahedral Mn active sites ($-Mn^{3+}_{(oct)}$) and

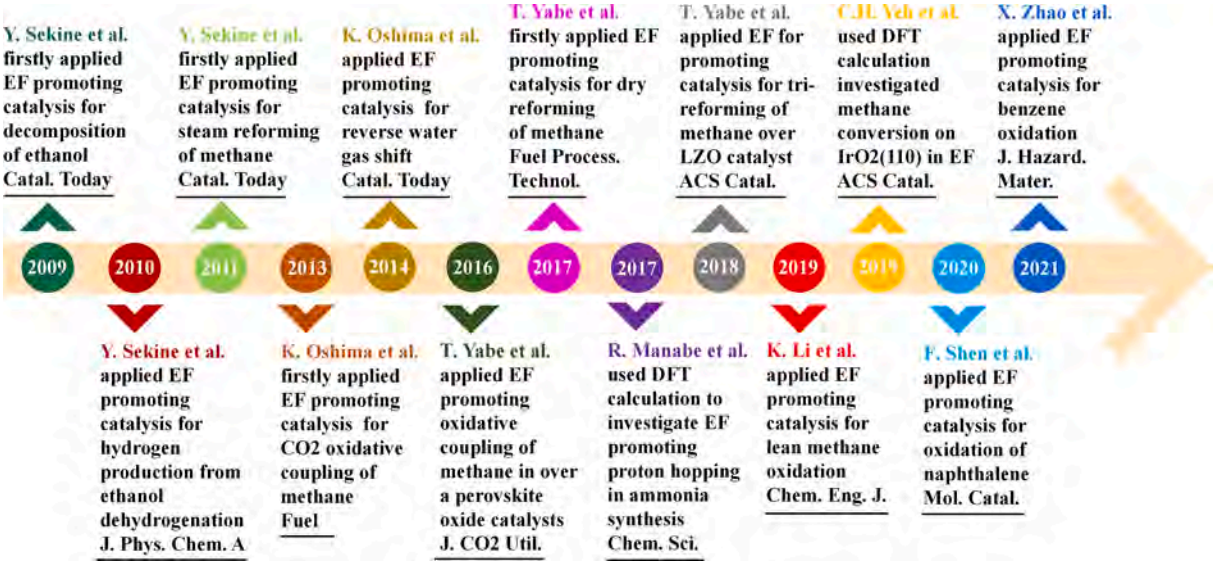

Fig. 2. Main events in the development of electric field promoting catalysis.

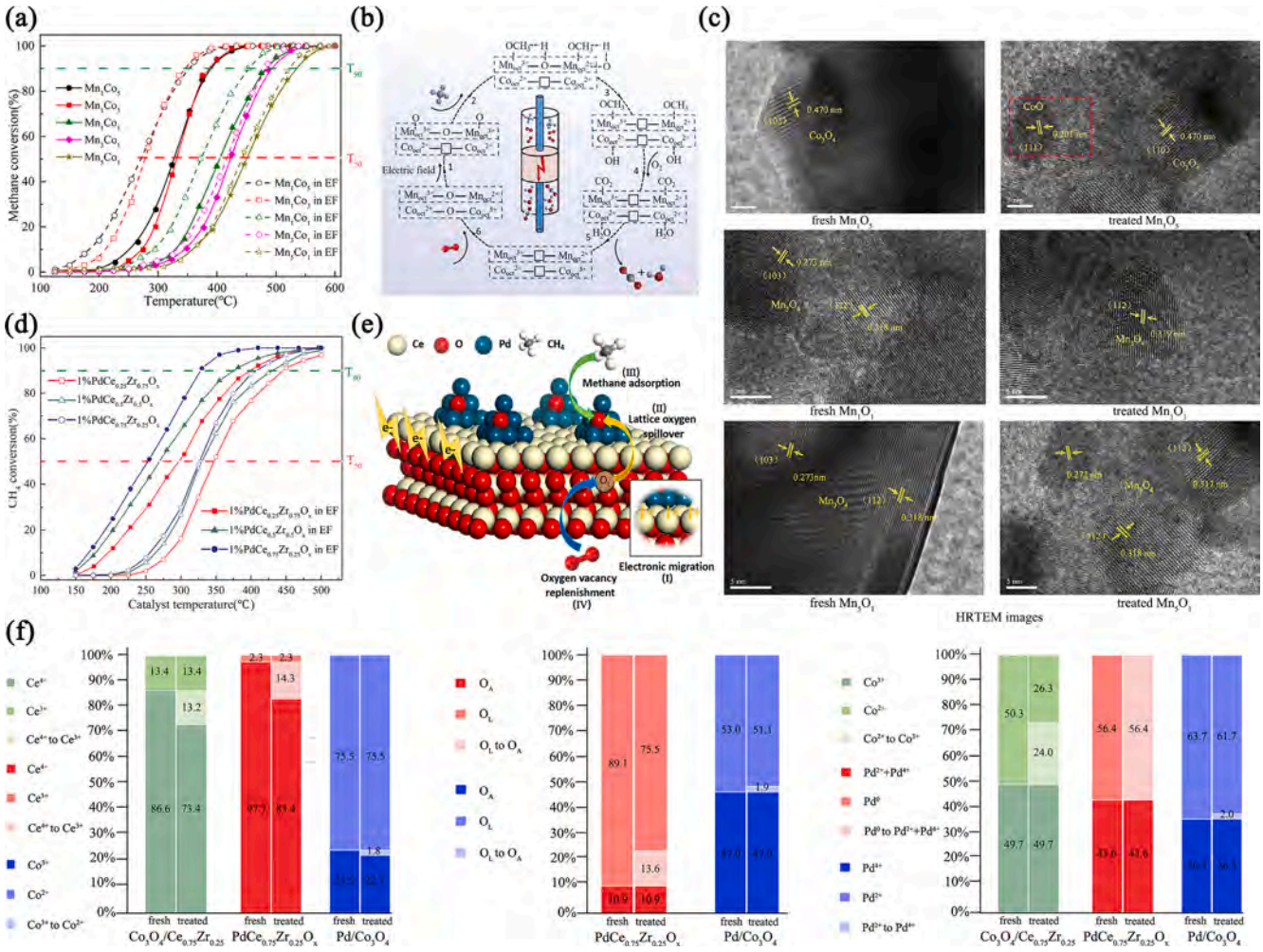

Fig. 3. (a) CH_4 conversion rate with/without EF, (b) mechanism of CH_4 catalytic oxidation in EF, and (c) high resolution transmission electron microscope (HRTEM) images of fresh and EF treated catalysts (over Mn_xCo_y) [58]. (d) CH_4 conversion rate with/without EF, and (e) Lattice oxygen transformation and methane surface adsorption in EF over $Pd/Ce_xZr_{1-x}O_y$ catalysts [97]. (f) Surface species valence change ratios by EF over Mn_xCo_y catalysts, $Pd/Ce_xZr_{1-x}O_y$ catalysts, and Pd/Co_4O_3 catalysts by X-ray photoelectron spectroscopy (XPS) [56].

oxygen migration for methane adsorption and oxidation. In HRTEM images, PdO (1 0 1) planes (0.26 nm d-spacing) were also observed on the ceria-based oxide grains surface of the treated sample [97], indicating that EF promoted the conversions of Pd^0 to PdO. Average crystal size (from TEM and XRD) grew smaller after EF was treated resulting from the re-dispersion of newly formed PdO clusters and crystal shrinkage for CeO reduction. It was also found by the work of D. Zagoraios et al. that the feedback trend to positive and negative voltages in specific reactant environments (methane/oxygen) was inconsistent, of monolithic metal film catalysts (Pd film) and dispersed metal particle catalysts (Pd/Co_3O_4), indicating a complex relationship between active site dispersibility, electric field properties, and oxygen species (O^{2-}) migration, and this complex interfacial reaction mechanism needs to be further investigated [55].

Surface atomic concentration and chemical valence states of the elements were detected by XPS, and the speculated oxygen species transformation process is shown in Fig. 3e, as followed: (I) Electron-obtaining reduction of Ce species and lattice oxygen energy storage; (II) lattice oxygen spillover and vacancy formation; (III) The methane chemisorption at surface oxygen sites; (IV) gaseous oxygen supplement in crystal bulk. After the baptism of electric fields, supporter metal cations oxides were reduced (Ce^{4+} to Ce^{3+}, Co^{3+} to Co^{2+}, and Zr^{4+} to Zr^{2+}), and the cations of loaded active metal were oxidized (Mn^{2+} to Mn^{3+}, Co^{2+} to Co^{3+}, Pd^0 and Pd^{2+} to Pd^{4+}) consequentially (Fig. 3f). Pd^0 on the surface has even been eliminated and converted into Pd^{2+} and Pd^{4+} (Pd^0/Pd^{n+} from 56.4 % to 0 %) over $PdCe_{0.75}Zr_{0.25}O_x$ in EF, indicating a great enhancement of reactivity and chemisorption at the active site. Furthermore, the ratios of adsorption oxygen in oxygen species ($O_A/(O_A + O_L)$) on EF treated sample acquired a few increasing implying in conversion from lattice oxygen to surface adsorbed oxygen. Overall, this low-temperature redox cycle in EF is consistent with the MvK model [97–99] instead of the E-R model of the conventional thermocatalysis.

Reference to structural parameters (Li et al.) from the surface differential diffraction studies (SSD) [100–103], exploiting XPS and In-situ DRIFT, the methane catalytic oxidation pathway on the Co_3O_4 {1 1 0} plane in the electric field has been verified [37], as followed:

(a) Non electric field: I. Gaseous oxygen adsorption and reaction sites generation → II. Methane chemisorption → III. Formate formation and conversion → IV. Carbonate generation → V. Carbon dioxide generation → VI. re-oxidation of Co^{2+} to Co^{3+}.

(b) Electric field: I. Electron transfer leads to lattice oxygen release and reaction sites generation→ II. Methane chemisorption → III. Carbonate generation → IV. Carbon dioxide generation → V. Lattice oxygen supplementation. The reaction cycle is accompanied by the generation of methoxy and hydroxyl groups, reduction of Co^{2+}, and dehydration, as shown in Fig. 4.

Methane chemisorption processes might be a pivotal session of the facilitation effect by incorporating electrons and energy. In Fig. 4b, none

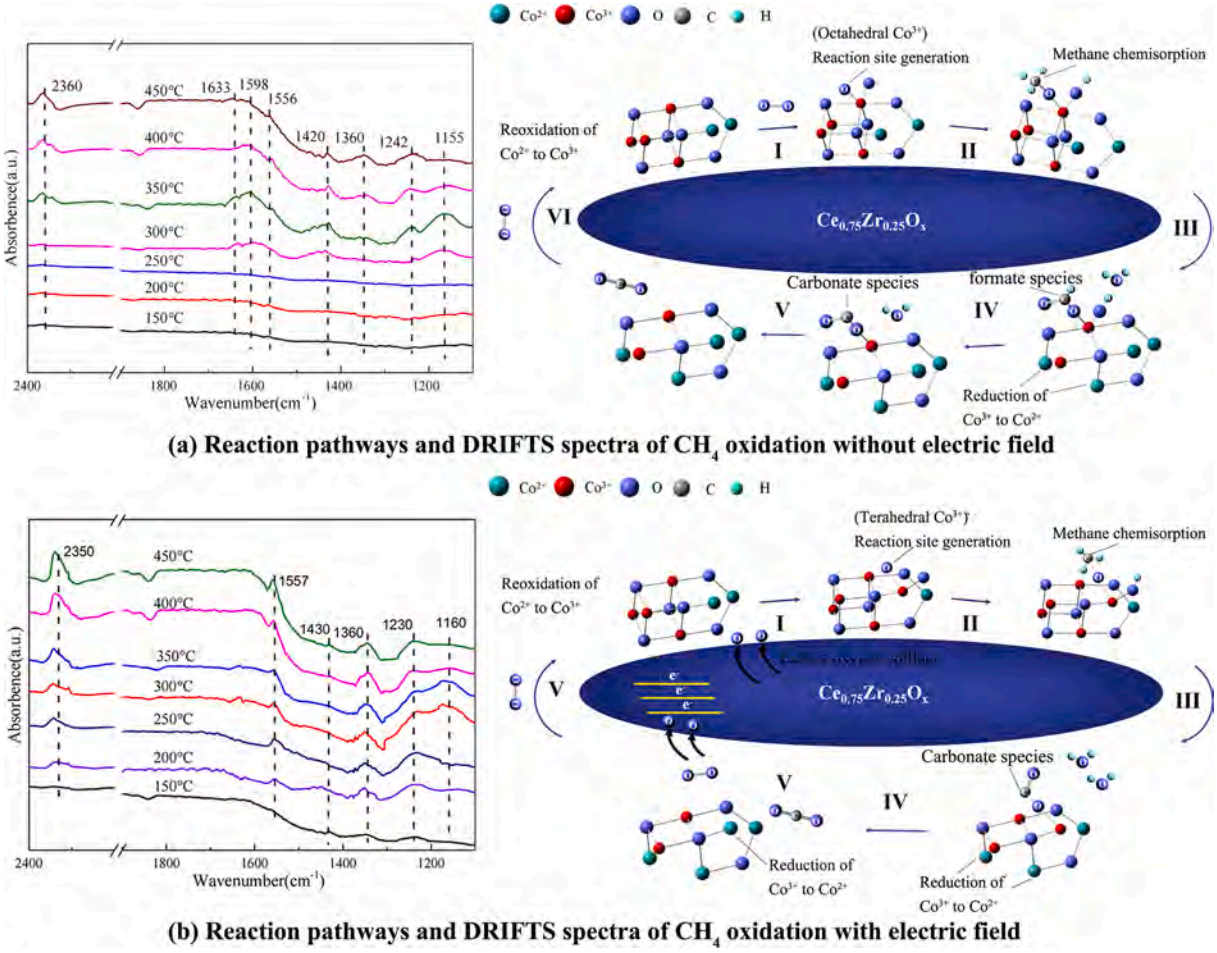

Fig. 4. In situ DRIFTS spectra and reaction pathway of CH_4 oxidation over Co-Ce-Zr catalyst: (a) without electric field and (b) with electric field [37].

of the dissociative and adsorptive O^{2-} ions (at 1160 cm^{-1} [104]) are detected, implying the active oxygen sites establishment actually mastered by lattice oxygen. The additional electrical energy broke the forceful stability of the original tetrahedral coordination Co^{2+}, instead of an octahedral one without EF (Fig. 4a), resulting in extra-activation of the connected oxygen sites, namely strengthening the oxidation capacity of Co-O. This type of activation in altering the location of oxygen site production shifted the reaction pathway and accelerated the transformation of certain intermediates. As shown in in-situ DRIFT spectra, there were no intricates to observe the absence of formates species retention (appeared at 1590 cm^{-1} and 1420 cm^{-1} [105]) in an electric field, indicating its rapid consumption for a subsequent generation of carbonate species. In short, the conversion of formates to carbonate species and chemisorption of methane considered as the two rate-determining steps were simultaneously driven forward by an electric field. Apart from the EF promoting mechanisms described above, the behaviour of hydroxyl groups was another influencing factor. Electronic intervention enhanced the reducibility of the metal species in the supporter, which accelerated dehydroxylation steps and prevented –OH attachment to the active site.

3.2. EF promoting catalytic oxidation of VOCs

The alleviation of volatile organic compounds (VOCs) emission has been an urgent assignment for the adverse impacts on human well-being and the environment [106]. The conventional catalytic combustion faced a challenge in achieving ring opening at low temperature, the complete removal of dilute BTEX (benzene, toluene, ethylbenzene, and p-xylene) almost above 200 °C [107–112]. Whereas, A wide variety of non-conventional technological accessions contributes to low-temperature catalysis, such as photo-catalysis, plasma-catalysis, microwave catalysis, and synergistic catalysis [113–116]. Lately, electric field promoting catalytic system was preliminarily extended into the VOCs removal field.

As shown in Table 2, for the removal conditions of hyper-dilute VOCs

Table 2
Performance of benzene catalytic oxidation under different conditions.

Catalysts	Feed conditions (N_2 balance)		T_{50}	T_{90}	GHSV	Ref.
	C_6H_6/$C_{10}H_8$(%)	O_2(%)	℃	℃	h^{-1}	
0.5% Pt/Al_2O_3	0.28 (C_6H_6)	20	132	143	32,000	[109]
1% Pt–0.5 %Pd/Al_2O_3	0.04 (C_6H_6)	20	212	237	60,000	[107]
1% Pt/TMS	0.04 (C_6H_6)	20	195	>200[a]	60,000	[111]
$Cu_{0.6}Mn$	0.1 (C_6H_6)	air	168	234	60,000	[112]
1% $PdCe_{0.25}Co_{0.75}$	0.1 (C_6H_6)	10	150[b]	175[b]	30,000	[59]
2% Pd/Co_3O_4	0.1 (C_6H_6)	10	175[b]	200[b]	60,000	[57]
1% Pt/$Ce_{0.75}Zr_{0.25}O_2$	0.1 (C_6H_6)	10	<75[b]	96.5[b]	30,000	[38]
NanoTiO$_2$/CeO_2	0.57 (C_6H_6)	5	160[c]	203[c]	48,000	[19]
2% Cu/$Ce_{0.55}Zr_{0.45}O_x$	0.01 (C_8H_{10})	10	173[b]	225[b]	60,000	[53]
Ag/CeO_2	0.012 (C_8H_{10})	10	175	> 220	175,000	[117]

[a] microwave irradiation catalysis.
[b] electric field promoting catalysis.
[c] photothermal catalysis.

(0.1 % for benzene, 0.01 % for naphthalene) and hypoxic (around 10 %), the electric field participation embodied unbeatable advantages compared with conventional catalytic combustion [107–109,112] or other novel systems [19,111,113–115], with T_{90} down to 96.5 °C and ΔT_{90} ($T_{90(non\text{-}EF)}$-$T_{90(EF)}$) up to 66.5 °C over Pt–Ce–Zr catalysts. The catalytic system stability is evaluated by 36 h continuous activity test in the reaction atmosphere at 150 °C (T_{100}), with virtually invisible conversion rate fluctuations [38]. For polycyclic aromatic hydrocarbons (PAHs) as naphthalene, non-noble metal catalysts can achieve the flat activity to noble one in an electric field [53,117]. The CO_2 selectivity, critical indicator for thorough purification, is even closed to 100 % when naphthalene converted completely.

The undeniable finding of XPS spectra is that the electron transfer enabling valence change and active oxygen sites formation is still the fundamental motivation of EF promoting catalytic oxidation of benzene and naphthalene. The lattice oxygen (O_L) escape from the supporter bulk combined with the Pt active component, greatly improves the oxidation capacity of the catalyst (Fig. 5). Because of the reaction complexity caused by the addition of the electric field and the benzene ring cleavage, the intermediate conversion of the entire reaction could not be described precisely. The characteristic peaks of intermediate products (formate, phenol, benzoquinone, maleic acid, and acetic acid) were detected successively in the In-situ DRIFTS spectrum during the heating-up process [38,57,59]. The speculated catalytic degradation pathway of benzene in/without EF was shown in Fig. 5. The apparent reasons for electric field promoting the oxidation of benzene at low temperature are as follows:

1. Compared to non-electric field conditions, multiple intermediates in electric fields are formed and transformed at lower temperatures, including benzene towards phenol conversion (100 °C down to 50℃) and benzoquinone to carbon dioxide conversion (125 °C down to 100℃).

2. In the EF promoting catalytic system, except for the above intermediate species, other peaks appeared after the conversion of benzoquinone and were identified as multiple esters and carboxylic acids, indicating a different oxidation path may exist.

Water resistance, the widely involved index, has a direct impact on catalytic activity for H_2O competitive adsorption with target. Dissociated hydroxyl group combine with active sites (M) to form $M(OH)_n$ hard-to-degrade, thus causing catalyst poisoning [97,118]. In hydrothermal resistance tests, water scarcely impacted benzene conversion over 1 % $Pt/Ce_{0.75}Zr_{0.25}$ catalyst with EF, 1–2 % conversion dropped with 10 vol % H_2O as well as 2–3 % with 20 vol% H_2O. The catalyst activity recovered thoroughly after water withdrawal [38]. No distinctive declines of P_{input} and ΔTOF* (turnover frequency/energy consumption) was observed as adding H_2O, indicating no significant humidity inhibition to the promoting effect of EF [97]. In a few reports, the electric field blocking water adsorption of the surface active site was an ambiguous concept to explain this property, the hydroxyl group may tend to attach to the supporter instead of loaded metal [58].

4. EF promoting catalysis for production of fuel or chemical feed gases

4.1. EF promoting oxidative coupling of methane

The adequate conversion is appreciated of low-price methane-dominated alkane to high value-added and transportable products in

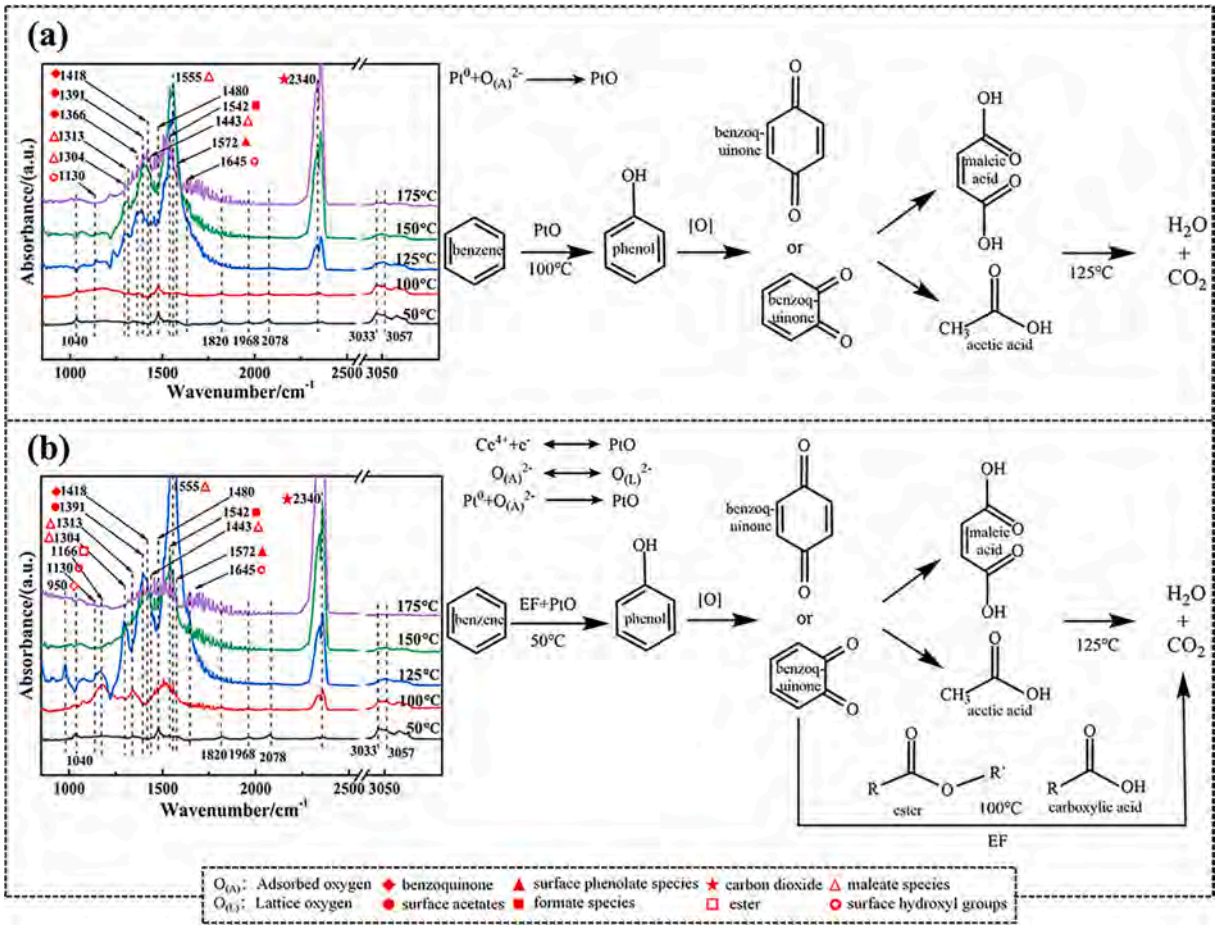

Fig. 5. (a) Catalytic degradation pathway of benzene without electric field and In situ DRIFTS spectra, (b) Catalytic degradation pathway of benzene in electric field and In situ DRIFTS spectra [38].

application [119–121]. A wide range of oxidative coupling of methane (OCM) reactions (as Eq. (2)) of catalytic and non-catalytic developed from the 1980s [122]. In traditional routes, OCM can obtain C_2 (ethane, ethylene, and acetylene) rather than C_3 by selective oxidation.

$$CH_4 + 1/2O_2 \rightarrow 1/2C_2H_4 + H_2O \quad \Delta H^0_{298} = -140.1\,kJ{\cdot}mol^{-1} \tag{2}$$

To improve the conversion from methane to the products (C_2 hydrocarbons), the hybrid systems of EF and catalysts were also applied to OCM. Using first-principles calculations with the Vienna ab initio simulation package (VASP) and X-ray absorption fine structure (XAFS) measurement, Ogo et al. argued that OCM is still originated from electric energy bringing lattice strain and electronic transport bringing valence change as shown in Fig. 6, and only the reaction intensity and end products varied from methane complete catalytic oxidation [34]. The absorption edge moves towards the higher-energy region in Ce K-edge spectra showed the valence change from Ce^{3+} to Ce^{4+} upon imposition of the electric field. In contrast, it is not be detected for the spectral offset of $La_2(WO_4)_3$ before and after the reaction (Fig. 6d). The calculated densities of states suggest that Ce^{3+} species in $Ce_2(WO_4)_3$ structure are oxidized to Ce^{4+} species in an electric field by the extraction of electrons from the Ce 4f orbitals near the Fermi level. Charge density difference plots confirm the electronic donation between ceria and oxygen. It leads to the lattice strain by introducing a positive charge, the decrease of Ce-O bond lengths and the increase of W-O bond lengths (Fig. 6d). Attendance beyond convention catalyst structures, core–shell interfaces of TiO_2(mc)/ZSM-5 has imposed the EF to promote OCM [123]. The extraordinary transformation from ethylene to propylene (ETP) was carried out at the Brønsted acid sites of the ZMS-5 core (Fig. 6f). There were inflection points for the CH_4 conversion, C_2 yield, and C_3 yield related to the temperature dependence (Fig. 6e) due to the decrease of TiO_2 semiconductivity and over-oxidation to CO or CO_2 at high temperatures respectively.

To restrain the sequential reaction, the technical routes included prolonging the beneficial reaction stage (from CH_4 to C_2) or intercepting the reaction process. The researchers hardly used noble-metal catalysts in favour of mixed metal oxide to prevent complete oxidation. According to recent investigations, a few strategies were recommended as incorporated electric fields and CO_2 substituting for O_2 oxidant, as CO_2-OCM (EF) [62,124,125], reaction as Eq. (3). The intercepting of this continuous chemical reaction is attributed to the low reactivity between ethylene (C_2) and carbon dioxide.

$$CH_4 + CO_2 \rightarrow 2C_2H_4 + 2CO \quad \Delta H^0_{298} = 142.1\,kJ{\cdot}mol^{-1} \tag{3}$$

CO_2-OCM requires thermal energy to meet CO-O bond dissociation (526.1 kJ mol^{-1}) and break thermodynamic equilibrium limitation, with reaction temperature reaching 1173 K. The electric energy filled

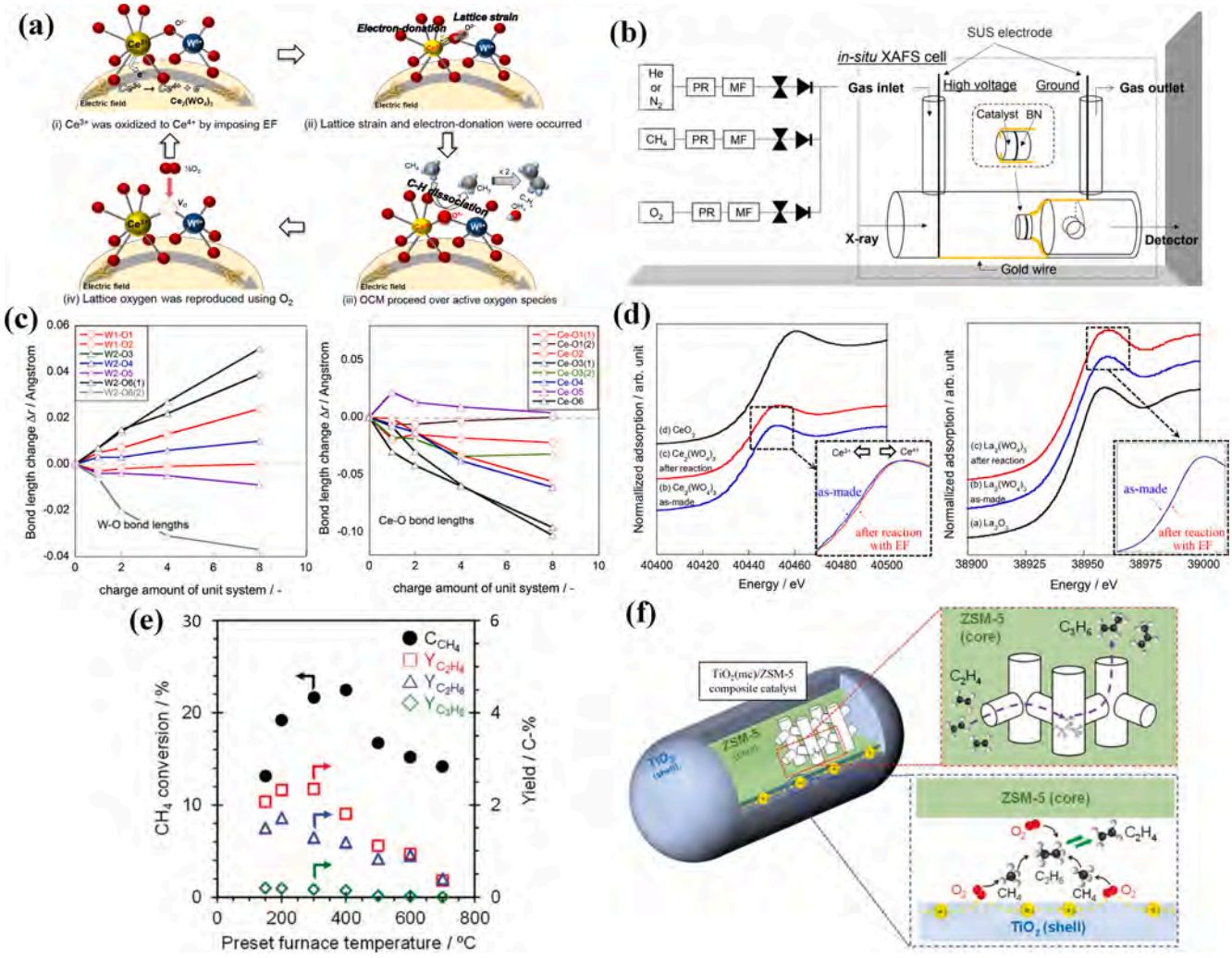

Fig. 6. (a) Inferred oxidative coupling mechanism in an electric field over $Ce_2(WO4)_3$. (b) Schematic image of in-situ XAFS cell for EF promoting catalysis. (c) Calculated bonds length change of W-O and Ce-O with different charge amounts. (d) Ex situ Ce K-edge XANES spectra of $Ce_2(WO_4)_3$ as-made, $Ce_2(WO_4)_3$ after reaction, CeO_2; $La_2(WO_4)_3$ as-made, $La_2(WO_4)_3$ after reaction, La_2O_3 [34]. (e) CH_4 conversion and $C_{2,3}$ yield and (f) reaction scheme of ETP over TiO2(mc)/ZSM-5_800 in EF [123].

the reaction activation energy, satisfying the reaction conditions of Eq. (5) at low temperatures. This low temperature prevents the direct conversion of the hydrocarbons to CO_2. Complicating the fact is that the involvement of an electric field leads to an added reaction, dry reforming of methane (DR) in Eq. (4).

$$CH_4 + CO_2 \rightarrow 2H_2 \quad \Delta H^0_{298} = 247.3\,kJ{\cdot}mol^{-1} \tag{4}$$

To secure C_2 conversion and selectivity for CO_2-OCM (EF), diverse ceramic semiconductor materials were investigated, including rare-earth oxides, alkali earth metal oxides, and perovskite oxides [60,126–128]. Tomohiro et al. [60] investigated implications for various substituted A sites or B sites of perovskite oxides ($LaAlO_3$ oxide) in CO_2-OCM (EF) and rated the $La_{0.7}Ca_{0.3}AlO_{3-\delta}$ as the most appropriate catalyst for C_2 yields up to 7.4 % at 348 K. This Ca doped ratio benefits carbon dioxide absorption without excess to form calcium carbonate. The conversion rate of CH_4 and CO_2 at 423 K is almost equivalent to the one in thermal catalysis at 1323 K, despite the existence disparity of OCM selectivity. Kinetic analysis exhibited the dependency on the carbon dioxide partial pressure (P_{CO2}) of C_2 generation rate in CO_2–OCM (EF), which affects the priority of the reactions. Dry steam reforming dominated the per unit power than methane oxidative coupling at lower P_{CO2}. As a result, increasing the current value or the contact time delivered conversion gains also inevitably affects OCM selectivity. Other alternative oxidants, such as N_2O and S_2 also used for promoting the light alkane partial oxidation, but no reports of concatenation with electric fields have been found so far [129–131].

4.2. EF promoting stream reforming of methane

Hydrogen had been utilized extensively in the chemical industries as an essential resource for petroleum refining and synthesizing ammonia and methanol [32,41,132,136]. H_2 was a surrogate power source to conventional fossil fuels with fuel cell spread implementation of transportation [137] and home appliances systems [138] for the high energy conversion and ignorable pollution emissions. The common H_2 production technology was steam reforming (SR) of methane, aromatic hydrocarbons [61], ethanol [133], and Dimethyl ether (DME) [71]. Taking SR of methane as an example, the reaction (Eq. (5)) are as follows [132].

$$CH_4 + 2H_2O \rightarrow 4H_2 + CO_2 \quad \Delta H^0_{298} = 164.9\,kJ{\cdot}mol^{-1} \tag{5}$$

The requirement for the reaction was endothermic (923–1123 K), being confronted with carbon deposition and catalyst deactivation. The ensuing complicated design of heat exchangers and heat resistance tubes also increased redundancy costs [32,132,133]. It concentrated in recent reports were cryogenic catalysts (Ni-based [139,140] or noble metal)

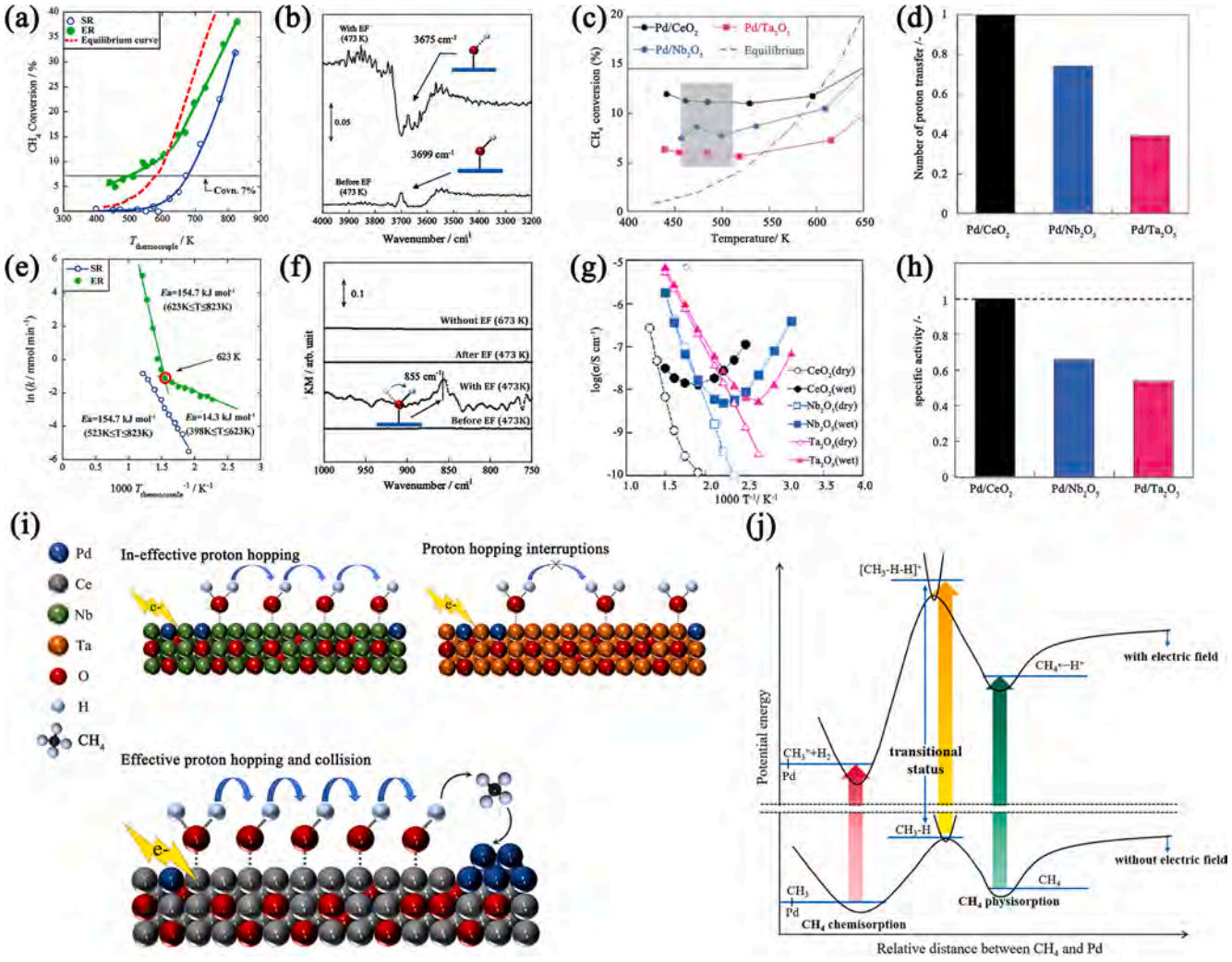

Fig. 7. (a) Comparison of methane conversions of ER, SR, and thermodynamic equilibrium. (e) Arrhenius plots of ER and SR at different temperatures, from ref. [32]. Operando-DRIFTS spectra before and after ER of (b) HO–H rotating peaks peaks and (f) O—H stretching. (c) methane conversion, (d) number of proton transport, (g) apparent electrical conductivity and (h) specific activity for different supporters (CeO_2, Nb_2O_5, and Ta_2O_5) [132]. (i) Schematic diagram of proton hopping level: effective, inefficient, and interrupt. (j) Schematic diagram of CH_4 dissociation adsorption and potential energy changes for ER.

and catalytic systems (NTP catalysis [141]) to solve this hardship. An advanced electric field synergistic steam reforming (ER) was obtained with adequate low-temperature conversion rates and hydrogen yields [7,132]. Results showed that the ER of methane conversions (7 %) at 473 K was equivalent to autothermal steam reforming (SR) at 673 K, encompassing some irreversible elementary steps over the limitation of the thermodynamic equilibrium curve (Fig. 7a). Arrhenius plots for ER and SR present a turnaround of apparent activation energy at 623 K, which brings out a new reaction pathway occurrence at a lower temperature in the electric field (Fig. 7e). Reaction rate dependence on partial pressure implied this perspective, described as followed by Eq. (6).

$$r = kP_{H_2O}^{\alpha}P_{CH_4}^{\beta} \tag{6}$$

The pressure exponential powers of water (α) and methane (β) changed from 0.1 and 0.9 to 0.7 and 0.25 respectively after the addition of the electric field. Similar to lean methane catalytic oxidation, the rate-determining stage of CH_4 chemosorption was wiped out and turned into an H_2O-related one in this reaction.

Researchers had further exploration associated these results with the water role on the protonic conductivity mentioned previously. Only with the electric field are the existence of adsorbed-water rotation bands (855 cm^{-1}) and the O—H bond length stretching (peak shifted from 3699 cm^{-1} to 3675 cm^{-1}) in *Operando*-DRIFTS spectra as Fig. 7b,f, which is proof of the appearance of surface proton conduction [7,132].

Multiple scenarios of kinetic isotope effects (KIE) measurement were using D_2O substitute for H_2O in SR and ER [7,132,134]. It resulted in a reaction rate constant ratio (k_H/k_D) less than unity in EF, proving the absence of the isotope-linked bond breakage in the rate-determining step. This "inverse" secondary KIE was indicated surface H^+ took a collision with CH_4 and promote the dissociate adsorption. The following formation of the transitional status (TS, as $[CH_3—H—H]^+$ configuration) raised the energy level and constructed an irreversible step towards $CH_{3ads}^+ + H_2$ (Fig. 7j). Moreover, another reason for the formation of energy barriers and promotion of adsorption was the low potential energy of CH_{3ads}^+ for electromigration brought by the positive charge.

The investigators hardly found valence state change of active metal sites (Pb) over CeO_2, Nb_2O_5, Ta_2O_5 supported catalyst during the ER [132,135]. Additionally, calculated TOF-s (turnover frequency/ the Pd surface area) and TOF-p (turnover frequency/Pd perimeter), through data results of CO pulse dosing and *Operando*-DRIFTS spectra reveal that the rate-determining stage might pertain to the supporter effect, due to turnover frequency value depends on the loaded palladium perimeter instead of the surface area in the EF [7,61,132,142].

$$T_{H+} = \sigma_{H+}/(\sigma_{H+} + \sigma_{e-}) = (\sigma_{wet} + \sigma_{dry}) + \sigma_{wet} \tag{7}$$

After evaluating hydroxyl amount by pyridine IR over above metal oxides supported catalyst, Torimoto et al. figured that the metal cation and oxygen species act respectively as Lewis acid and base sites contribute to H_2O adsorption on the oxide surface [132]. Conductivity discrepancy may cause gaps of electrical energy accessing and affect the water molecule adsorption capacity (as the proton donator), thus protonic hopping manifested as an effective, ineffective, and interruption over Pd/CeO_2, Pd/Nb_2O_5, Pd/Ta_2O_5 catalyst (Fig. 7i). The proton transport number (T_{H+}) was calculated by Eq. (7) and Eq. (1), according to the apparent conductivity of EIS measurement (Fig. 7g). T_{H+} were 1.0 (Pd/CeO_2), 0.74 (Pd/Nb_2O_5), and 0.34 (Pd/Ta_2O_5) at 473 K (Fig. 7d), highly compatible with normalized activity (Fig. 7h). This reaffirms that catalyst supporter conductivity affects the number of proton transport and thus the activity of methane steam reforming.

4.3. EF promoting ammonia synthesis

Ammonia is a highly sought-after material of hydrogen storage for simple liquefaction and superior H-storage capacity [143]. Nitrogen molecules exhibit dissociative inert for a strong triple bond (945 kJ mol^{-1}), hence the conditions for industrial ammonia synthesis require high temperature (>350 °C) and high pressure (>10 MPa) [144]. Compared with the conventional iron-modified catalyst in the Fritz-Haber Process, the Ru-based catalyst takes on more attention for up to tenfold ammonia yield (in the case of abundant B_5-type step sites) [145]. In addition to the enhanced catalytic activity through the acquisition of electrons from alkaline earth metal oxide promoters, the incorporation of electric fields has become emerging facilitation for ammonia synthesis. This application obtained a remarkably high ammonia yield of production rate as high as 31 mmol $g_{cat}^{-1}h^{-1}$ at 0.9 MPa with a stable duration of 500 h [31,146–148]. Experimental results show that protons govern the ammonia synthesis reaction in the EF through two mechanisms, the "dissociative mechanism" and the "associative mechanism" [31]. N_2 dissociation and N_2H formation are the rate-determining steps for these two mechanisms, as Fig. 8c. DFT calculation reveals this reaction energy (*Er*) variations of N_2 dissociation and N_2H formation reactions as Fig. 8e. Under mainly considering Ru (10-11) dominant facets (higher area ratio as Fig. 8a,b), the reaction energy of N_2 dissociation reactions increases slightly, but the *Er* of N_2H formation decreases to negative values, which indicates that the process of N_2H formation changes from endothermic to an exothermic in the electric field. This explains the ammonia synthetic activation energy decrease obtained in EF from the Arrhenius plot (Fig. 8f) of theoretical calculations and experiments. We obtained a remarkably high ammonia yield, with an ammonia production rate as high as 31 mmol gcat1 h1 at 0.9 MPa, which is still in the kinetically controlled region. Seen in some other EF promoting catalysis was this proton hopping (Fig. 8d), including methylcyclohexane dehydrogenation, and dry reforming, merely with a different proton source.

5. Comprehensive understanding of mechanisms

The electric field exhibits the nature of material and energy through electronic transfer and electrical energy in multiple catalytic reactions, which induce a shared mechanism framework of the multiple reactions (Fig. 9). As followed, the electricity changes the metal oxides microstructure of bond length and bond angle over heterogeneous catalysts, thereby driving lattice strain interaction (as Ce–O and W–O bonds [34]). Some species converted their valence by the repeated electronic gain-loss (as the behavior of Ce and Co in lean methane catalytic oxidation [37]), enhancing the redox ability of various elements in the catalyst. Our group argues that this synergistic effect among electronic transfer, electrical energy, and catalysts act as the underlying cause for a suite of the characteristic phenomenon, including the highlighted proton hopping, oxygen species migration, active site increase, and the rate-determining step modifying.

The superior cryogenic activity is noteworthy for a practical application, brought by modifying reaction paths and rate-determining steps in this system. Particularly the adsorption steps of reactive molecules mentioned earlier, represented by methane dissociative chemisorption, were accelerated by the collision or bonding action of energetically acquired protons or lattice oxygen respectively. Furthermore, the energy consumption benefit in the system is on account of the electric field facilitating the original reaction process (such as the conversion of formate to carbonate), rather than generating extra active species(ROS) and free radicals against the reactants directly as plasma catalysis. This auxiliary catalysis in EF barely leads to refractory intermediates emerging, thus improving its CO_2 selectivity of complete oxidation. Of course, some of the other intrinsic mechanisms by which systemic advantages gain a foothold have not been well studied, including excellent hydrothermal resistance, stability, and product selectivity.

6. Conclusion and outlook

The electric field promoting catalytic system was proposed for

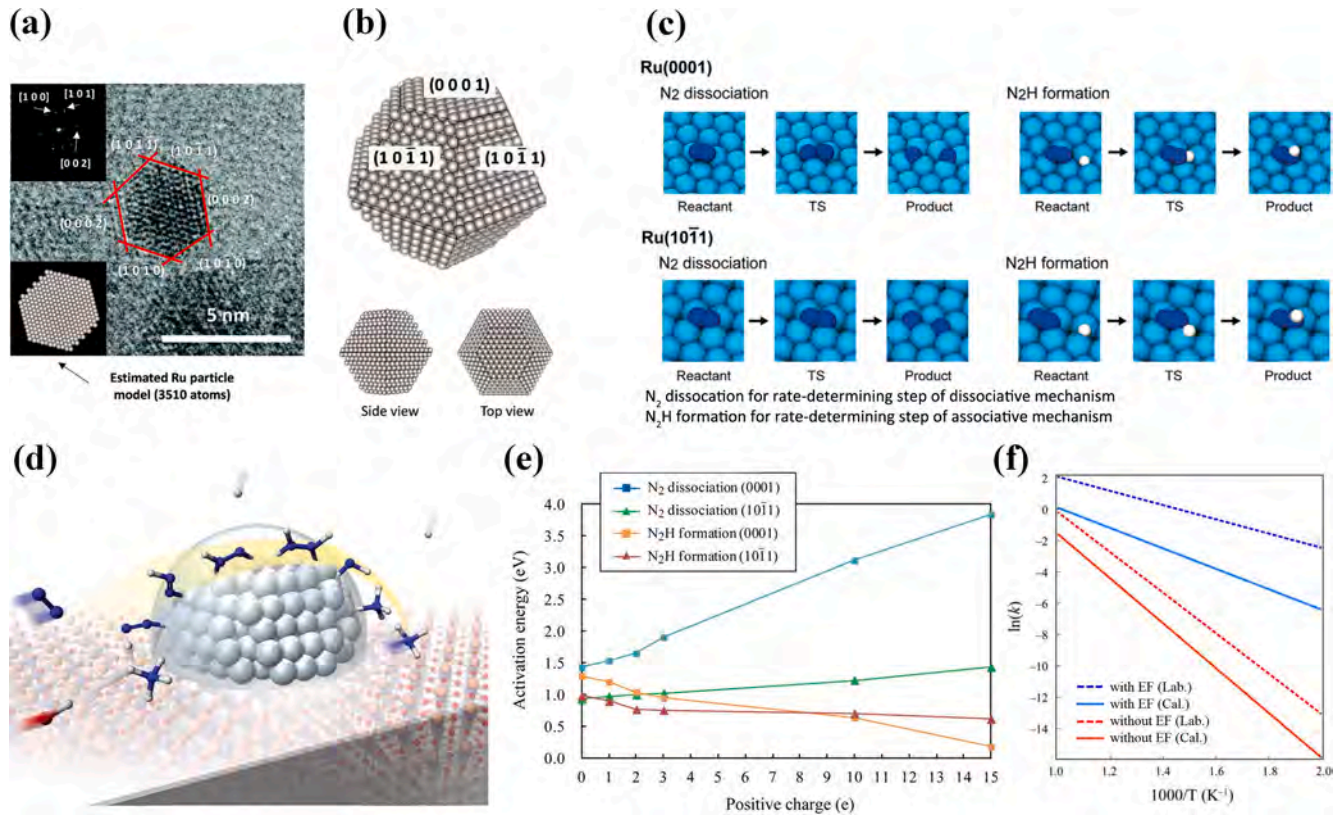

Fig. 8. (a) TEM images of a $SrZrO_3$ supported Ru particles. (b) Predicted Ru particle model and the facets. (c) Optimized structures of the reactant state, transition state (TS) and product state of the N_2 dissociation and N_2H formation reactions over Ru (0001) and Ru (10-11) (d) Schematic mechanism of the EF promoting ammonia synthesis. (e) the Reaction energy (*Er*) of the N_2 dissociation and N_2H formation on Ru (10-11). (f) Arrhenius plot for ammonia synthesis (with/without EF) over Ru (10-11), from ref. [31].

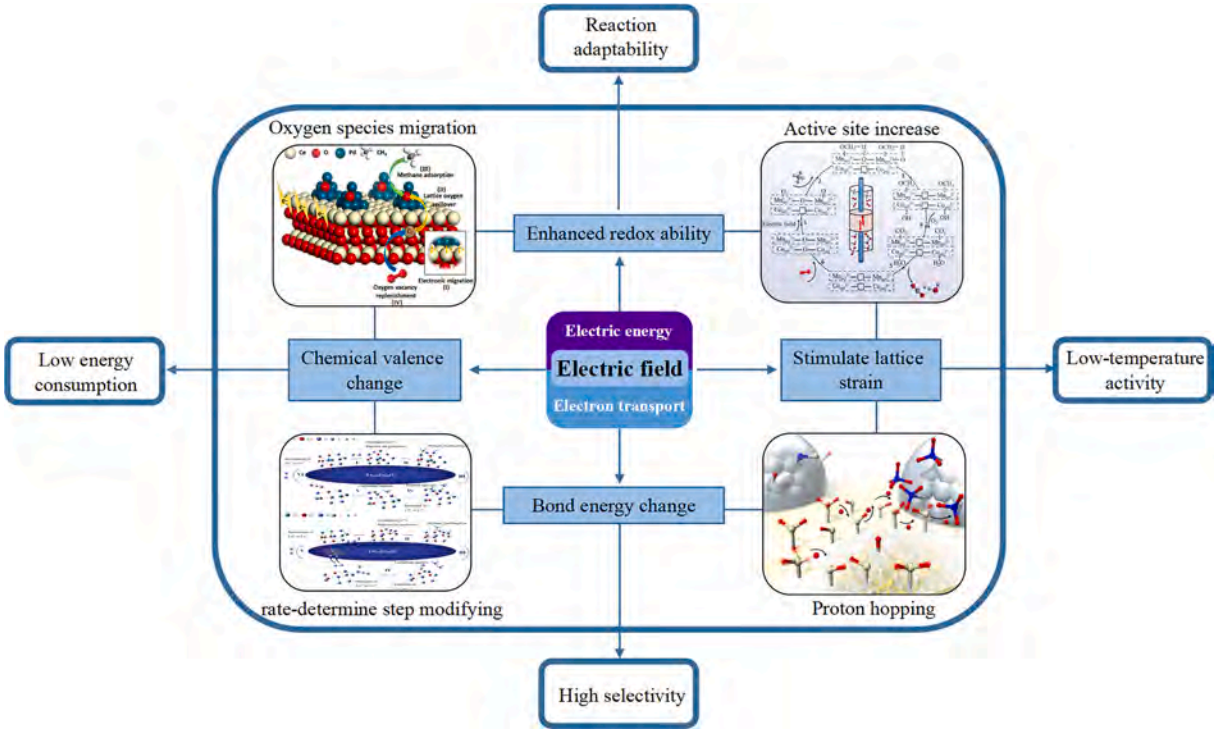

Fig. 9. Mechanistic arrangement of EF promoting catalytic system: the core processes; the distinctive feature phenomena; outstanding advantages.

decomposition, synthesis, reforming, oxidative coupling reactions of chemical feed gas and fuel gas Initially. As global environmental issues stand out, researchers have been turning their attention to the harmful gaseous abatement. It seems to us the synergistic effects among electron, electrical energy, and catalysts undertake an intrinsic motivation of several system merits. Some characteristic phenomenon constantly impinges on the original reaction processes, widening out a larger gap over conventional catalysis in cryogenic reaction activity, energy consumption, and product selectivity. However, many issues between laboratory research and commercialization need to be explored and resolved, as follows:

First the research scope and application scenarios need to be expanded for this catalytic system, especially in the reaction type, catalyst structure, and target reactants. The prospects of extending this system to other fields were predictable for their outstanding merits in energy consumption, reaction temperature, selectivity, and adaptability. At least, it is worthy to conduct experimental extension in catalytic oxidation of concerned hazardous gases, including toluene, xylene, formaldehyde, acetaldehyde, and so on. Though metallic elemental loading and doping are subjected to the conductive constraint, the catalyst structures can be modified particularly for selective catalytic oxidation and multi-reactant synergistic conversion.

Second the reaction mechanism imperfections were reflected in past research, process descriptions show some fragmentation, although most researchers have established this aspect as a research focus. In ER, it is deserved exploration whether the lattice oxygen takes a role of thrusters on the subsequent adsorbed methane oxidation, as similar in complete catalytic oxidation. In aromatic hydrocarbons catalytic oxidation, the promoting process of the electric field onto ring fracture is not figured out. The nitty–gritty related to mechanism also should be further attention, such as the interaction for hydroxyl groups behavior and water-resistance in EF promoting catalytic reactions.

Third some evaluative indicators need to be established before this system turns into a pilot scale experiment. Energy conversion efficiency (considering the thermal release) and TOF* [97] could be meaningful parameters for evaluating the system. The stability and deactivation analysis (roman spectroscopy) of the catalyst in this system should be included in the fundamental parameters and set a reasonable stability testing time threshold.

In summary, the electric field promoting catalysis constitutes an attractive solution onto the hazardous gas degradation, greenhouse gases abatement and resources & energy crisis, which satisfy the demanding requirements of energy consumption and gaseous pollutant treatment. In future research, developing competitive catalysts adapted to the electric field coupling action and achieving system scale-up stabilization were the critical link for practical engineering applications.

Declaration of Competing Interest

The authors declare that they have no known competing financial interests or personal relationships that could have appeared to influence the work reported in this paper.

Data availability

Data will be made available on request.

Acknowledgements

This work was financially supported by the National Key Research and Development Program of China (2016YFC0204100) and the Key Research and Development Program of Hunan Province in China (2018SK2032).

References

[1] P.E. Brockway, A. Owen, L.I. Brand-Correa, L. Hardt, Estimation of global final stage energy-return-on-investment for fossil fuels with comparison to renewable energy sources, Nat. Energy 4 (7) (2019) 612–621.
[2] F. Pietrapertosa, C. Cosmi, M. Macchiato, M. Salvia, V. Cuomo, Life cycle assessment, externe and comprehensive analysis for an integrated evaluation of the environmental impact of anthropogenic activities, Renew. Sust. Energ. Rev. 13 (5) (2009) 1039–1048.
[3] K. Zheng, L. Tan, Y. Sun, Y. Wua, Z. Duan, Y. Xua, C. Gao, Impacts of climate change and anthropogenic activities on vegetation change: evidence from typical areas in China, Ecol. Indic. 126 (2021), 107648.
[4] S. Shi, Z. Sun, C. Bao, T. Gao, Y.H. Hu, The special route toward conversion of methane to methanol on a fluffy metal-free carbon nitride photocatalyst in the presence of H_2O_2, Int. J. Energy Res. 44 (4) (2020) 2740–2753.
[5] M. Li, Z. Sun, H.H. Yun, Thermo-photo coupled catalytic CO_2 reforming of methane: a review, Chem. Eng. J. 428 (2022), 131222.
[6] R.A. Dias, C.R. Mattos, J.A.P. Balestieri, The limits of human development and the use of energy and natural resources, Energy Policy 34 (9) (2006) 1026–1031.
[7] Y. Hisai, Q. Ma, T. Qureishy, T. Watanabe, T. Higo, T. Norby, Y. Sekine, Enhanced activity of catalysts on substrates with surface protonic current in an electrical field–a review, Chem. Commun. 57 (2021) 5737–5749.
[8] Y. Sekine, R. Manabe, Reaction mechanism of low-temperature catalysis by surface protonics in an electric field, Faraday Discuss. 229 (2021) 341–358.
[9] S. Ogo, Y. Sekine, Catalytic reaction assisted by plasma or electric field, Chem. Rec. 17 (2017) 726–738.
[10] Y. Xu, Z. Zhou, M. Zou, Y. Liu, Y. Zheng, Y. Yang, S. Lan, J. Lan, C.W. Nan, Y. H. Lin, Multi-field driven hybrid catalysts for CO_2 reduction: progress, mechanism and perspective, Mater. Today 54 (2022) 225–246, https://doi.org/10.1016/j.mattod.2022.02.005.
[11] B. Zhu, L. Zhang, M. Li, Y. Yan, X. Zhang, Y. Zhu, High-performance of plasma-catalysis hybrid system for toluene removal in air using supported Au nanocatalysts, Chem. Eng. J. 381 (2020), 122599.
[12] Y. Yan, J. Lin, T. Xu, B. Liu, K. Huang, L. Qiao, S. Liu, J. Cao, S.C. Jun, Y. Yamauchi, J. Qi, Atomic-level platinum filling into Ni-vacancies of dual-deficient NiO for boosting electrocatalytic hydrogen evolution, Adv. Energy Mater. 12 (2022) 2200434.
[13] F. Cai, D. Gao, H. Zhou, G. Wang, T. He, H. Gong, S. Miao, F. Yang, J. Wang, X. Bao, Electrochemical promotion of catalysis over Pd nanoparticles for CO_2 reduction, Chem. Sci. 8 (2017) 2569–2573.
[14] D. Panayotov, A. Frenkel, J.R. Morris, Catalysis and photocatalysis by nanoscale Au/TiO_2: perspectives for renewable energy, ACS Energy Lett. 2 (5) (2017) 1223–1331.
[15] B.M. da Costa Filho, G.V. Silva, R.A.R. Boaventura, M.M. Dias, J.C.B. Lopes, V.J. P. Vilar, Ozonation and ozone-enhanced photocatalysis for VOC removal from air streams: process optimization, synergy and mechanism assessment, Sci. Total Environ. 687 (2019) 1357–1368.
[16] L. Li, K. Yan, J. Chen, T. Feng, F. Wang, J. Wang, Z. Song, C. Ma, Fe-rich biomass derived char for microwave-assisted methane reforming with carbon dioxide, Sci. Total Environ. 657 (2019) 1357–1367.
[17] C. Yan, M. Zhong, J. He, X. Lu, Y. Zhang, L. Liu, Efficient degradation of trimethylamine in gas phase by petal-shaped Co-MoS_2 catalyst in the photo-electrochemical system, Chem. Eng. J. 405 (2021), 127034.
[18] T. Zadi, M. Azizi, N. Nasrallah, A. Bouzaza, R. Maachi, D. Wolbert, S. Rtimi, A. A. Assadi, Indoor air treatment of refrigerated food chambers with synergetic association between cold plasma and photocatalysis: process performance and photocatalytic poisoning, Chem. Eng. J. 382 (2020), 122951.
[19] M. Zeng, Y. Li, M. Mao, J. Bao, L. Ren, Synergetic Effect between photocatalysis on TiO_2 and Thermocatalysis on CeO_2 for gas-phase oxidation of benzene on TiO_2/CeO_2 nanocomposites, ACS Catal. 5 (6) (2015) 3278–3286.
[20] M. Stoukides, C.G. Vayenas, The effect of electrochemical oxygen pumping on the rate and selectivity of ethylene oxidation on polycrystalline silver, J. Catal. 70 (1) (1981) 137–146.
[21] A.H. Khoja, M. Tahir, N.A.S. Amin, Evaluating the performance of a Ni catalyst supported on La_2O_3-$MgAl_2O_4$ for dry reforming of methane in a packed bed dielectric barrier discharge plasma reactor, Energy Fuels 33 (2019) 11630–11647.
[22] Y. Guo, X. Liao, J. He, W. Ou, D. Ye, Effect of manganese oxide catalyst on the dielectric barrier discharge decomposition of toluene, Catal. Today 153 (3) (2010) 176–183.
[23] B. Wang, Y. Xiong, Y. Han, J. Hong, Y. Zhang, J. Li, F. Jing, W. Chu, Preparation of stable and highly active Ni/CeO_2 catalysts by glow discharge plasma technique for glycerol steam reforming, Appl. Catal., B 249 (2019) 257–265.
[24] P. Chawdhury, Y. Wang, D. Ray, S. Mathieu, N. Wang, J. Harding, F. Bin, X. Tu, C. Subrahmanyam, Promising plasma-catalytic approach towards single-step methane conversion to oxygenates at room temperature, Appl. Catal., B 284 (2021), 119735.
[25] Y. Zhang, W. Chu, W. Cao, C. Luo, X. Wen, A plasma-activated Ni/α-Al_2O_3 catalyst for the conversion of CH_4 to syngas, Plasma Chem. Plasma Process. 20 (1) (2000) 137–144.
[26] Y. Wang, M. Craven, X. Yu, J. Ding, P. Bryant, J. Huang, X. Tu, Plasma-enhanced catalytic synthesis of ammonia over a Ni/Al_2O_3 catalyst at near-room temperature: insights into the importance of the catalyst surface on the reaction mechanism, ACS Catal. 9 (2019) 10780–10793.

[27] S. Li, X. Dang, X. Yu, G. Abbas, Q. Zhang, L. Cao, The application of dielectric barrier discharge non-thermal plasma in VOCs abatement: a review, Chem. Eng. J. 388 (2020), 124275.
[28] K.H.R. Rouwenhorst, Y. Engelmann, K. Veer, R.S. Postma, A. Bogaerts, L. Lefferts, Plasma-driven catalysis: green ammonia synthesis with intermittent electricity, Green Chem. 22 (2020) 6258–6287.
[29] Y. Sekine, M. Tomioka, M. Matsukata, E. Kikuchi, Catalytic degradation of ethanol in an electric field, Catal. Today 146 (2009) 183–187.
[30] F. Che, J.T. Gray, S. Ha, N. Kruse, S.L. Scott, J.-S. McEwen, Elucidating the roles of electric fields in catalysis: a perspective, ACS Catal. 8 (2018) 5153–5174.
[31] R. Manabe, H. Nakatsubo, A. Gondo, K. Murakami, S. Ogo, H. Tsuneki, M. Ikeda, A. Ishikawa, H. Nakai, Y. Sekine, Electrocatalytic synthesis of ammonia by surface proton hopping, Chem. Sci. 8 (2017) 5434.
[32] R. Manabe, S. Okada, R. Inagaki, K. Oshima, S. Ogo, Y. Sekine, Surface protonics promotes catalysis, Sci. Rep. 6 (2016) 38007.
[33] K. Takise, A. Sato, K. Murakami, S. Ogo, S. Kado, Y. Sekine, Irreversible catalytic methylcyclohexane dehydrogenation by surface protonics at low temperature, RSC Adv. 9 (11) (2019) 5918–5924.
[34] S. Ogo, H. Nakatsubo, K. Iwasaki, A. Sato, K. Murakami, T. Yabe, A. Ishikawa, H. Nakai, Y. Sekine, Electron-hopping brings lattice strain and high catalytic activity in the low-temperature oxidative coupling of methane in an electric field, J. Phys. Chem. C 122 (2018) 2089–2096.
[35] C.H. Yeh, T.M.L. Pham, S. Nachimuthu, J.C. Jiang, Effect of external electric field on methane conversion on IrO_2(110) surface: a density functional theory study, ACS Catal. 9 (2019) 8230–8242.
[36] F. Che, S. Ha, J.-S. McEwe, Elucidating the field influence on the energetics of the methane steam reforming reaction: a density functional theory study, Appl. Catal., B 195 (2016) 77–89.
[37] K. Li, K. Liu, D. Xu, H. Ni, F. Shen, T. Chen, B. Guan, R. Zhan, Z. Huang, H. Lin, Lean methane oxidation over $Co_3O_4/Ce_{0.75}Zr_{0.25}$ catalysts at low temperature: synergetic effect of catalysis and electric field, Chem. Eng. J. 369 (2019) 660–671.
[38] X. Zhao, D. Xu, Y. Wang, Z. Zheng, K. Li, Y. Zhang, R. Zhan, H. Lin, Electric field assisted benzene oxidation over Pt-Ce-Zr nano-catalysts at low temperature, J. Hazard. Mater. 407 (2021), 124349.
[39] T. Yabe, K. Mitarai, K. Oshima, S. Ogo, Y. Sekine, Low-temperature dry reforming of methane to produce syngas in an electric field over La-doped Ni/ZrO_2 catalysts, Fuel Process. Technol. 158 (2017) 96–103.
[40] K. Oshima, K. Tanaka, T. Yabe, Y. Sekine, Catalytic oxidative coupling of methane with a dark current in an electric field at low external temperature, Int. J. Plasma Environ. Sci. Technol. 6 (3) (2012) 266–271.
[41] K. Oshima, T. Shinagawa, Y. Nogami, R. Manabe, S. Ogo, Y. Sekine, Low temperature catalytic reverse water gas shift reaction assisted by an electric field, Catal. Today 232 (2014) 27–32.
[42] Y. Sekine, M. Haraguchi, M. Matsukata, E. Kikuchi, Low temperature steam reforming of methane over metal catalyst supported on $Ce_xZr_{1-x}O_2$ in an electric field, Catal. Today 171 (2011) 116–125.
[43] H.H. Berger, Contact resistance and contact resistivity, J. Electrochem. Soc. 119 (4) (1972) 507.
[44] R. Ye, J. Zhao, B.B. Wickemeyer, F.D. Toste, Foundations and strategies of the construction of hybrid catalysts for optimized performances, Nat. Catal. 1 (2018) 318–325.
[45] T. Yu, J. Jiao, P. Song, W. Nie, C. Yi, Q. Zhang, P. Li, Recent progress in continuous-flow hydrogenation, ChemSusChem 13 (2020) 1–19.
[46] Y. hong, W. Zhang, Q. Xu, X.T. Wu, Q.L. Zhu, Pore surface engineering of metal–organic frameworks for heterogeneous catalysis, Coord Chem Rev 376 (2018) 248–276.
[47] T. Arai, S. Iimura, J. Kim, Y. Toda, S. Ueda, H. Hosono, Chemical design and example of transparent bipolar semiconductors, J. Am. Chem. Soc. 139 (47) (2017) 17175–17180.
[48] Y.A. Bratashevskii, A.Y. Zakharov, Y.M. Ivanchenko, Forbidden band width change in semiconductor substitution alloys, Solid State Commun. 15 (11) (1974) 1777–1779.
[49] W. Wang, B. Xu, P. Gao, W. Zhang, Y. Sun, Electrical and dielectric properties of $HoMnO_3$ ceramics, Solid State Commun. 177 (2014) 7–9.
[50] R. Sakai, K. Murakami, Y. Mizutani, Y. Tanaka, S. Hayashi, A. Ishikawa, T. Higo, S. Ogo, H. Tsuneki, H. Nakai, Y. Sekine, Key factor for the anti-arrhenius low-temperature heterogeneous catalysis induced by H migration: H coverage over support, ACS Omega 5 (12) (2020) 6846–6851.
[51] X. Zhao, Y. Wang, Z. Zheng, Y. Zhang, K. Li, T. Chen, D. Guo, H. Cao, R. Zhan, H. Lin, Comparative study on properties of Pd–Ce–Zr catalysts synthesized by flame spray pyrolysis and solution combustion: application for methane catalytic oxidation in electric field, Appl. Surf. Sci. 566 (2021), 150536.
[52] K. Sugiura, S. Ogo, K. Iwasaki, T. Yabe, Y. Sekine, Low-temperature catalytic oxidative coupling of methane in an electric field over a Ce–W–O catalyst system, Sci. Rep. 6 (2016) 25154.
[53] F. Shen, K. Li, D. Xu, R. Yan, T. Chen, R. Zhan, H. Lin, Electric field promoted oxidation of naphthalene over $Cu/Ce_{0.55}Zr_{0.45}O_x$ catalysts at low temperature, Mol. Catal. 476 (2019), 110536.
[54] Y. Sekine, K. Yamagishi, Y. Nogami, R. Manabe, Low temperature catalytic water gas shift in an electric field, Catal Lett. 146 (2016) 1423–1428.
[55] D. Zagoraios, A. Athanasiadi, I. Kalaitzidou, S. Ntais, A. Katsaounis, A. Caravaca, P. Vernoux, C.G. Vayenas, Electrochemical promotion of methane oxidation over nanodispersed Pd/Co_3O_4 catalysts, Catal. Today 355 (2020) 910–920.
[56] K. Liu, K. Li, D. Xu, H. Lin, Z. Huang, Catalytic combustion of lean methane assisted by electric field over Pd/Co_3O_4 catalysts at low temperature, J. Shanghai Jiao Tong Univ. (Sci.) 23 (Sup. 1) (2018) 8–17.
[57] F. Shen, K. Li, X. Dejun, X. Li, X. Zhao, T. Chen, R. Zhan, H. Lin, Electric field promoted complete oxidation of benzene over $PdCe_xCo_y$ catalysts at low temperature, Catal. 9 (2019) 1071.
[58] K. Li, D. Xu, K. Liu, H. Ni, F. Shen, T. Chen, B. Guan, R. Zhan, Z. Huang, H. Lin, Catalytic combustion of lean methane assisted by an electric field over Mn_xCo_y catalysts at low temperature, J. Phys. Chem. C 123 (2019) 10377–10388.
[59] F. Shen, K. Li, X. Zhao, X. Li, T. Chen, R. Zhan, T. Zhao, H. Lin, Low temperature oxidation of benzene over Pd/Co_3O_4 catalysts in the electric field, Catal Lett. 151 (2021) 67–77.
[60] T. Yabe, Y. Kamite, K. Sugiura, S. Ogo, Y. Sekine, Low-temperature oxidative coupling of methane in an electric field using carbon dioxide over Ca-doped $LaAlO_3$ perovskite oxide catalysts, J. CO_2 Util. 20 (2017) 156–162.
[61] K. Takise, A. Sato, K. Muraguchi, S. Ogo, Y. Sekine, Steam reforming of aromatic hydrocarbon at low temperature in electric field, Appl. Catal., A 573 (2019) 56–63.
[62] K. Oshima, K. Tanaka, T. Yabe, E. Kikuchi, Y. Sekine, Oxidative coupling of methane using carbon dioxide in an electric field over La–ZrO_2 catalyst at low external temperature, Fuel 107 (2013) 879–881.
[63] R. Manabe, S. Stub, T. Norby, Y. Sekine, Evaluating surface protonic transport on cerium oxide via electrochemical impedance spectroscopy measurement, Solid State Commun 270 (2018) 45–49.
[64] Z. Zuo, Y. Fu, A. Manthiram, Novel Blend Membranes based on acid-base interactions for fuel cells, Polymers 4 (2012) 1627–1644.
[65] N. Agmon, The Grotthuss mechanism, Chem. Phys. Lett. 244 (1995) 456–462.
[66] Y. Yan, J. Lin, T. Liu, B. Liu, B. Wang, L. Qiao, J. Tu, J. Cao, J. Qi, Corrosion behavior of stainless steel-tungsten carbide joints brazed with AgCuX (X = In, Ti) alloys, Corros. Sci. 200 (2022), 110231.
[67] S.Ø. Stub, E. Vøllestad, T. Norby, Mechanisms of protonic surface transport in porous oxides: example of YSZ, J. Phys. Chem. C 121 (23) (2017) 12817–12825.
[68] T. Ano, S. Tsubaki, A. Liu, M. Matsuhisa, S. Fujii, K. Motokura, W.J. Chun, Y. Wada, Probing the temperature of supported platinum nanoparticles under microwave irradiation by in situ and operando XAFS, Commun. Chem. 3 (2020) 86.
[69] M. Kosaka, T. Higo, S. Ogo, J.G. Seo, S. Kado, K. Imagawa, Y. Sekine, Low-temperature selective dehydrogenation of methylcyclohexane by surface protonics over Pt/anatase-TiO_2 catalyst, Int. J. Hydrogen Energy 45 (1) (2020) 738–743.
[70] K. Takise, A. Sato, S. Ogo, J.G. Seo, K. Imagawa, S. Kado, Y. Sekine, Low-temperature selective catalytic dehydrogenation of methylcyclohexane by surface protonics, RSC Adv. 9 (2019) 27743–27748.
[71] X.Y. Xu, H. Guo, C. Zhao, Probing the electric field effect on the catalytic performance of Mn-doped graphene to CO oxidation, J. Phys. Chem. C 121 (2017) 27983–27991.
[72] R. Inagaki, R. Manabe, Y. Hisai, Y. Kamite, T. Yabe, S. Ogo, Y. Sekine, Steam reforming of dimethyl ether promoted by surface protonics in an electric field, Int. J. Hydrogen Energy 43 (2018) 14310–14318.
[73] C. Panaritis, Y.M. Hajar, L. Treps, C. Michel, E.A. Baranova, S.N. Steinmann, Demystifying the atomistic origin of the electric field effect on methane oxidation, J. Phys. Chem. Lett. 11 (2020) 6976–6981.
[74] F. Sun, W. Zeng, Electric field effects on hydrogen/methane oxidation: a reactive force field based moleculardynamics study, Int. J. Hydrogen Energy 45 (2020) 20194–20199.
[75] X. Huang, C. Tang, J. Li, L.C. Chen, J. Zheng, P. Zhang, J. Le, R. Li, X. Li, J. Liu, Y. Yang, J. Shi, Z. Chen, M. Bai, H.L. Zhang, H. Xia, J. Cheng, Z.Q. Tian, W. Hong, Electric field induced selective catalysis of single-molecule reaction, Sci. Adv. 5 (2019) eaaw3072.
[76] M. Akamatsu, N. Sakai, S. Matile, Electric-field-assisted anion–π catalysis, J. Am. Chem. Soc. 139 (19) (2017) 6558–6561.
[77] R. Ramanan, D. Danovich, D. Mandal, S. Shaik, Catalysis of methyl transfer reactions by oriented external electric fields: are gold−thiolate linkers innocent? J. Am. Chem. Soc. 140 (2018) 4354–4362.
[78] Q. Li, P. He, J. Jarvis, A. Bhattachary, X. Mao, A. Wang, G.M. Bernard, V. K. Michaelis, H. Zeng, L. Liu, H. Song, Catalytic co-aromatization of methane and heptane as an alkane model compound over Zn-Ga/ZSM-5: a mechanistic study, Appl. Catal., B 236 (2018) 13–24.
[79] J. Xu, A. Zheng, X. Wang, G. Qi, J. Su, J. Du, Z. Gan, J. Wu, W. Wang, F. Deng, Room temperature activation of methane over Zn modified H-ZSM-5 zeolites: insight from solid-state NMR and theoretical calculations, Chem. Sci. 3 (2012) 2932–2940.
[80] J.H. Lunsford, Catalytic conversion of methane to more useful chemicals and fuels: a challenge for the 21st century, Catal. Today 63 (2000) 165–174.
[81] D. Fino, N. Russo, G. Saracco, V. Specchia, Supported Pd-perovskite catalyst for CNG engines exhaust gas treatment, Prog. Solid. State Ch. 35 (2) (2007) 501–511.
[82] J. Fernández, P. Marín, F.V. Díez, S. Ordóñez, Coal mine ventilation air methane combustion in a catalytic reverse flow reactor: influence of emission humidity, Fuel Process. Technol. 133 (Supplement C) (2015) 202–209.
[83] J. Yin, S. Su, X. Yu, J.-S. Bae, Y. Jin, A. Villella, M. Jara, M. Ashby, M. Cunnington, M. Loney, Site trials and demonstration of a novel pilot ventilation air methane mitigator, Energy Fuels 34 (8) (2020) 9885–9893.
[84] S. Su, J. Agnew, Catalytic combustion of coal mine ventilation air methane, Fuel 85 (9) (2006) 1201–1210.

[85] E. Díaz, J. Fernández, S. Ordóñez, N. Canto, A. González, Carbon and ecological footprints as tools for evaluating the environmental impact of coal mine ventilation air, Ecol. Ind. 18 (2012) 126–130.

[86] P. Goyal, Sidhartha, Present scenario of air quality in Delhi: a case study of CNG implementation, Atmos. Environ. 37 (38) (2003) 5423–5431.

[87] C. Li, W. Li, K. Chen, A.T. Ogunbiyi, Z. Zhou, Q. Duan, F. Xue, Highly active Pd catalysts supported on surface-modified cobalt-nickel mixed oxides for low temperature oxidation of lean methane, Fuel 279 (2020), 118372.

[88] K. Murata, J. Ohyama, Y. Yamamoto, S. Arai, A. Satsuma, Methane combustion over Pd/Al_2O_3 catalysts in the presence of water: effects of Pd particle size and alumina crystalline phase, ACS Catal. 10 (15) (2020) 8149–8156.

[89] Y. Ding, Q. Wu, B. Lin, Y. Guo, Y. Guo, Y. Wang, L. Wang, W. Zhan, Superior catalytic activity of a Pd catalyst in methane combustion by fine-tuning the phase of ceria-zirconia support, Appl. Catal., B 266 (2020), 118631.

[90] X. Guo, G. Zhi, X. Yan, G. Jin, X. Guo, P. Brault, Methane combustion over Pd/ZrO_2/SiC, Pd/CeO_2/SiC, and $Pd/Zr_{0.5}Ce_{0.5}O_2$/SiC catalysts, Catal. Commun. 12 (10) (2011) 870–874.

[91] Y. Lei, W. Li, Q. Liu, Q. Lin, X. Zheng, Q. Huang, S. Guan, X. Wang, C. Wang, F. Li, Typical crystal face effects of different morphology ceria on the activity of Pd/CeO_2 catalysts for lean methane combustion, Fuel 233 (2018) 10–20.

[92] J.Y. Luo, M. Meng, X. Li, X.G. Li, Y.Q. Zha, T.D. Hu, Y.N. Xie, J. Zhang, Mesoporous Co_3O_4–CeO_2 and Pd/Co_3O_4–CeO_2 catalysts: synthesis, characterization and mechanistic study of their catalytic properties for low-temperature CO oxidation, J. Catal. 254 (2) (2008) 310–324.

[93] L.F. Liotta, G.D. Carlo, G. Pantaleo, G. Deganello, E.M. Borla, M. Pidria, Honeycomb supported Co_3O_4/CeO_2 catalyst for CO/CH_4 emissions abatement: effect of low Pd–Pt content on the catalytic activity, Catal. Commun. 8 (3) (2007) 299–304.

[94] L.H. Xiao, K.P. Sun, X.L. Xu, X.N. Li, Low-temperature catalytic combustion of methane over Pd/CeO_2 prepared by deposition precipitation method, Catal. Commun. 6 (2005) 796–801.

[95] G. Ercolino, A. Grodzka, G. Grzybek, P. Stelmachowski, S. Specchia, A. Kotarba, The effect of the preparation method of Pd-doped cobalt spinel on the catalytic activity in methane oxidation under lean fuel conditions, Top. Catal. 60 (2017) 333–341.

[96] M. Cargnello, J.J.D. Jaén, J.C.H. Garrido, K. Bakhmutsky, T. Montini, J.J. C. Gámez, R.J. Gorte, P. Fornasiero, Exceptional activity for methane combustion over modular Pd@ CeO_2 subunits on functionalized Al_2O_3, Science 337 (2012) 713–717.

[97] K. Li, K. Liua, H. Ni, B. Guan, R. Zhan, Z. Huang, H. Lin, Electric field promoted ultra-lean methane oxidation over Pd-Ce-Zr catalysts at low temperature, Mol. Catal. 459 (2018) 78–88.

[98] T.R. Baldwin, R. Burch, Catalytic combustion of methane over supported palladium catalysts: I. Alumina supported catalysts, Appl. Catal., A 66 (1) (1990) 337–358.

[99] O. Demoulin, M. Navez, P. Ruiz, Investigation of the behaviour of a Pd/γ-Al_2O_3 catalyst during methane combustion reaction using in situ DRIFT spectroscopy, Appl. Catal., A 295 (1) (2005) 59–70.

[100] X. Xie, Y. Li, Z.Q. Liu, M. Haruta, W. Shen, Low-temperature oxidation of CO catalysed by Co_3O_4 nanorods, Nature 458 (7239) (2009) 746–749.

[101] J. Ziókowski, Y. Barbaux, Identification of sites active in oxidation of butene-1 to butadiene and CO_2 on CO_3O_4 in terms of the crystallochemical model of solid surfaces, J. Mol. Catal. 67 (2) (1991) 199–215.

[102] D.K. Chlebda, P.J. Jodlowski, R.J. Jedrzejczyk, J. Lojewska, Generalised two-dimensional correlation analysis of the Co, Ce, and Pd mixed oxide catalytic systems for methane combustion using in situ infrared spectroscopy, Spectrochim. Acta., A 192 (2018) 202–210.

[103] J.P. Jacobs, A. Maltha, J.G.H. Reintjes, J. Drimal, V. Ponec, H.H. Brongersma, The surface of catalytically active spinels, J. Catal. 147 (1) (1994) 294–300.

[104] J. Li, X. Liang, S. Xu, J. Hao, Catalytic performance of manganese cobalt oxides on methane combustion at low temperature, Appl. Catal., B 90 (1) (2009) 307–312.

[105] C. Cao, A. Bourane, J.R. Schlup, K.L. Hohn, In situ IR investigation of activation and catalytic ignition of methane over Rh/Al_2O_3 catalysts, Appl. Catal., A 344 (1) (2008).

[106] W.B. Li, J.X. Wang, H. Gong, Catalytic combustion of VOCs on non-noble metal catalysts, Catal. Today 148 (2009) 81–87.

[107] H.S. Kim, T.W. Kim, H.L. Koh, S.H. Lee, B.R. Min, Complete benzene oxidation over Pt-Pd bimetal catalyst supported on γ-alumina: Influence of Pt-Pd ratio on the catalytic activity, Appl. Catal., A 280 (2005) 125–131.

[108] S. Mo, S. Li, J. Li, S. Peng, J. Chen, Y. Chen, Promotional effects of Ce on the activity of MnAl oxide catalysts derived from hydrotalcites for low temperature benzene oxidation, Catal. Commun. 87 (2016) 102–105.

[109] Z. Chen, J. Mao, R. Zhou, Preparation of size-controlled Pt supported on Al_2O_3 nanocatalysts for deep catalytic oxidation of benzene at lower temperature, Appl. Surf. Sci. 465 (2019) 15–22.

[110] P. Petrova, T. Tabakova, G. Munteanu, R. Zanella, M. Tsvetkov, L. Ilieva, Gold catalysts on Co-doped ceria for complete benzene oxidation: Relationship between reducibility and catalytic activity, Catal. Commun. 36 (2013) 84–88.

[111] X. Liu, S. Ding, S. Shigenobu, H. Hojo, H. Einaga, Catalyst design of Pt/TiO_2 microsphere for benzene oxidation under microwave irradiation, Catal. Today 376 (15) (2021) 285–291.

[112] W. Tang, X. Wu, S. Li, X. Shan, G. Liu, Y. Chen, Co-nanocasting synthesis of mesoporous Cu-Mn composite oxides and their promoted catalytic activities for gaseous benzene removal, Appl. Catal., B 162 (2015) 110–121.

[113] X. Zeng, B. Li, R. Liu, X. Li, T. Zhu, Investigation of promotion effect of Cu doped MnO_2 catalysts on ketone-type VOCs degradation in a one-stage plasma-catalysis system, Chem. Eng. J. 384 (2020), 123362.

[114] R. Liu, H. Song, B. Li, X. Li, T. Zhu, Simultaneous removal of toluene and styrene by non-thermal plasma-catalysis: effect of VOCs interaction and system configuration, Chemosphere 263 (2021), 127893.

[115] M. Zhang, S. Cai, J. Li, E.A. Elimian, J. Chen, H. Jia, Ternary multifunctional catalysts of polymeric carbon nitride coupled with Pt-embedded transition metal oxide to enhance light-driven photothermal catalytic degradation of VOCs, J. Hazard. Mater. 412 (2021), 125266.

[116] W. Gao, X. Zhang, X. Su, F. Wang, Z. Liu, B. Liu, J. Zhan, H. Liu, Y. Sang, Construction of bimetallic Pd-Ag enhanced $AgBr/TiO_2$ hierarchical nanostructured photocatalytic hybrid capillary tubes and devices for continuous photocatalytic degradation of VOCs, Chem. Eng. J. 346 (2018) 77–84.

[117] M. Liu, X. Wu, S. Liu, Y. Gao, Z. Chen, Y. Ma, R. Ran, D. Weng, Study of Ag/CeO_2 catalysts for naphthalene oxidation: Balancing the oxygen availability and oxygen regeneration capacity, Appl. Catal., B 219 (2017) 231–240.

[118] Y. Guo, Y. Gao, X. Li, G. Zhuang, K. Wang, Y. Zheng, D. Sun, J. Huang, Q. Li, Catalytic benzene oxidation by biogenic Pd nanoparticles over 3D-ordered mesoporous CeO_2, Chem. Eng. J. 362 (2019) 41–52.

[119] A. Sato, S. Ogo, K. Kamata, Y. Takeno, T. Yabe, T. Yamamoto, S. Matsumura, M. Hara, Y. Sekine, Ambient-temperature oxidative coupling of methane in an electric field by a cerium phosphate nanorod catalyst, Chem. Commun. 55 (2019) 4019.

[120] P. Schwach, X. Pan, X. Bao, Direct conversion of methane to value-added chemicals over heterogeneous catalysts: challenges and prospects, Chem. Rev. 117 (2017) 8487–8520.

[121] A.I. Olivos-Suarez, A. Szecsenyi, E.J.M. Hensen, J. Ruiz-Martinez, E.A. Pidko, J. Gascon, Strategies for the direct catalytic valorization of methane using heterogeneous catalysis: challenges and opportunities, ACS Catal. 6 (2016) 2965–2981.

[122] T. Ito, J.H. Lunsford, Synthesis of ethylene and ethane by partial oxidation of methane over lithium-doped magnesium oxide, Nature 314 (1985) 721–722.

[123] Q. Han, A. Tanaka, M. Matsumoto, A. Endo, Y. Kubota, S. Inagak, Conversion of methane to C_2 and C_3 hydrocarbons over TiO_2/ZSM-5 core–shell particles in an electric field, RSC Adv. 9 (2019) 34793.

[124] Y. Wang, Y. Ohtsuka, Mn-based binary oxides as catalysts for the conversion of methane to C_2 hydrocarbons with carbon dioxide as oxidant, Appl. Catal., A 219 (2001) 183–193.

[125] K. Asami, T. Fujita, K. Kusakabe, Y. Nishiyama, Y. Ohtsuka, Conversion of methane with carbon dioxide into C_2 hydrocarbons over metal oxides, Appl. Catal., A 126 (1995) 245–255.

[126] V.R. Choudhary, V.H. Rane, Acidity/basicity of rare-earth oxides and their catalytic activity in oxidative coupling of methane to C_2-hydrocarbons, J. Catal. 130 (1991) 411–422.

[127] N. Mimura, I. Takahara, M. Inaba, M. Okamoto, K. Murata, High-performance Cr/H-ZSM-5 catalysts for oxidative dehydrogenation of ethane to ethylene with CO_2 as an oxidant, Catal. Commun. 3 (2002) 257–262.

[128] N. Mimura, M. Okamoto, H. Yamashita, S.T. Oyama, K. Murata, Oxidative dehydrogenation of ethane over Cr/ZSM-5 catalysts using CO_2 as an oxidant, J. Phys. Chem. B 110 (2006) 21764–21770.

[129] E.V. Kondratenko, M. Cherian, M. Baerns, D. Su, R. Schlcgl, X. Wang, I.E. Wachs, Oxidative dehydrogenation of propane over V/MCM-41 catalysts: comparison of O_2 and N_2O as oxidants, J. Catal. 234 (2005) 131–142.

[130] M.B. Ward, M.J. Lin, J.H. Lunsford, The oxidative dehydrogenation of ethane by nitrous oxide over molybdenum oxide supported on silica gel, J. Catal. 50 (1977) 306–318.

[131] A.M. Arinaga, M.C. Ziegelski, T.J. Marks, Alternative oxidants for the catalytic oxidative coupling of methane, Angew. Chem. 133 (2021) 10596–10609.

[132] M. Torimoto, S. Ogo, Y. Hisai, N. Nakano, A. Takahashi, Q. Ma, J. Gil Seo, H. Tsuneki, T. Norby, Y. Sekine, Support effects on catalysis of low temperature methane steam reforming, RSC Adv. 10 (2020) 26418.

[133] Y. Sekine, M. Haraguchi, M. Tomioka, M. Matsukata, E. Kikuchi, Low-temperature hydrogen production by highly efficient catalytic system assisted by an electric field, J. Phys. Chem. A 114 (2010) 3824–3833.

[134] S. Okada, R. Manabe, R. Inagaki, S. Ogo, Y. Sekine, Methane dissociative adsorption in catalytic steam reforming of methane over Pd/CeO_2 in an electric field, Catal. Today 307 (2018) 272–276.

[135] A. Takahashi, R. Inagaki, M. Torimoto, Y. Hisai, T. Matsuda, Q. Ma, J. Gil Seo, T. Higo, H. Tsuneki, S. Ogo, T. Norby, Y. Sekine, Effects of metal cation doping in CeO_2 support on catalytic methane steam reforming at low temperature in an electric field, RSC Adv. 10 (2020) 14487.

[136] T. Yabe, K. Yamada, T. Oguri, T. Higo, S. Ogo, Y. Sekine, Ni−Mg supported catalysts on low-temperature electrocatalytic tri-reforming of methane with suppressed oxidation, ACS Catal. 8 (2018) 11470–11477.

[137] W. Wu, K.B. Liew, S. Abbas, M.A. Raza, J.J. Hwang, S.B. Yang, Z. Li, Exergy-based modular design of an on-board MeOH-to-H_2 processor for fuel cell vehicles, Int. J. Hydrogen Energy 45 (2020) 19880–19890.

[138] S. Cao, K. Alanne, Technical feasibility of a hybrid on-site H_2 and renewable energy system for a zero-energy building with a H_2 vehicle, Appl. Energy 158 (2015) 568–583, https://doi.org/10.1016/j.apenergy.2015.08.009.

[139] M.A. Nieva, M.M. Villaverde, A. Monzon, T.F. Garetto, A.J. Marchi, Steam-methane reforming at low temperature on nickel-based catalysts, Chem. Eng. J. 235 (2014) 158–166.

[140] Q. Zhao, Y. Wang, Y. Wang, L. Li, W. Zeng, G. Li, C. Hu, Steam reforming of CH_4 at low temperature on Ni/ZrO_2 catalyst: Effect of H_2O/CH_4 ratio on carbon

deposition, Int. J. Hydrogen Energy 45 (2020) 14281–14292, https://doi.org/10.1016/j.ijhydene.2020.03.112.
[141] Y. Xing, Z. Liu, R.A. Couttenye, W.S. Willis, S.L. Suib, P.T. Fanson, H. Hirata, M. Ibe, Generation of hydrogen and light hydrocarbons for automotive exhaust gas purification: Conversion of n-hexane in a PACT (plasma and catalysis integrated technologies) reactor, J. Catal. 250 (2007) 67.
[142] T. Yabe, K. Yamada, K. Murakami, K. Toko, K. Ito, T. Higo, S. Ogo, Y. Sekine, Role of electric field and surface protonics on low-temperature catalytic dry reforming of methane, ACS Sustainable Chem. Eng. 7 (2019) 5690–5697.
[143] K. Kishida, M. Kitano, Y. Inoue, M. Sasase, T. Nakao, T. Tada, H. Abe, Y. Niwa, T. Yokoyama, T. Yokoyama, M. Hara, H. Hosono, Large oblate hemispheroidal ruthenium particles supported on calcium amide as efficient catalysts for ammonia decomposition, Chem. Eur. J. 24 (2018) 7976–7984.
[144] S. Kanbara, M. Kitano, Y. Inoue, T. Yokoyama, M. Hara, H. Hosono, Mechanism switching of ammonia synthesis over Ru-loaded electride catalyst at metal−insulator transition, J. Am. Chem. Soc. 137 (2015) 14517–14524.
[145] N. Morlanés, W. Almaksoud, R.K. Rai, S. Ould-Chikh, M.M. Ali, B. Vidjayacoumar, B.E. Al-Sabban, K. Albahily, J.M. Basset, Development of catalysts for ammonia synthesis based on metal phthalocyanine materials, Catal Sci. Technol. 10 (2020) 844–852.
[146] R. Sakai, K. Murakami, Y. Mizutani, Y. Tanaka, S. Hayashi, A. Ishikawa, T. Higo, S. Ogo, H. Tsuneki, H. Nakai, Y. Sekine, Agglomeration suppression of a Fe-supported catalyst and its utilization for low-temperature ammonia synthesis in an electric field, ACS Omega 5 (12) (2020) 6846–6851.
[147] K. Murakami, Y. Tanaka, R. Sakai, Y. Hisai, S. Hayashi, Y. Mizutani, T. Higo, S. Ogo, J.G. Seo, H. Tsunekia, Y. Sekine, Key factor for the anti-arrhenius low-temperature heterogeneous catalysis induced by H^+ migration: H^+ coverage over support, Chem. Commun. 56 (2020) 3365.
[148] K. Murakamia, Y. Tanakaa, R. Sakaia, K. Tokoa, K. Itoa, A. Ishikawab, T. Higoa, T. Yabea, S. Ogoa, M. Ikedac, H. Tsunekic, H. Nakaid, Y. Sekine, The important role of N_2H formation energy for low-temperature ammonia synthesis in an electric field, Catal. Today 351 (2020) 119–124.